

**Surface Wave Characterization of Wind Turbine Sites in Jamaica,
using the MASW and Side Scatter Methods**

by

Shelby L. Peterie
Sarah L. Morton
Amanda J. Livers
J. Jordan Nolan
Anthony Hoch
Brett Judy
Yao Wang
Julian Ivanov
Richard D. Miller

Kansas Geological Survey
1930 Constant Avenue, Campus West
Lawrence, Kansas 66047-3726

final report to

Chris Kopchynski
Bill W. Kussmann

Barr Engineering Company
4700 West 77th Street
Minneapolis, MN 55435-4803

February 26, 2015

KGS Open-file Report 2015-27

The Kansas Geological Survey makes no warranty or representation, either express or implied, with regard to the data, documentation, or interpretations or decisions based on the use of this data including the quality, performance, merchantability, or fitness for a particular purpose. Under no circumstances shall the Kansas Geological Survey be liable for damages of any kind, including direct, indirect, special, incidental, punitive, or consequential damages in connection with or arising out of the existence, furnishing, failure to furnish, or use of or inability to use any of the database or documentation whether as a result of contract, negligence, strict liability, or otherwise. This study was conducted in complete compliance with ASTM Guide D7128-05. All data, interpretations, and opinions expressed or implied in this report and associated study are reasonably accurate and in accordance with generally accepted scientific standards.

Surface Wave Characterization of Wind Turbine Sites in Jamaica, using the MASW and Side Scatter Methods

Summary

Surface seismic data were acquired at eleven sites in St. Elizabeth Parish, Jamaica. The objectives of the project were to identify potential anomalies that may represent weak zones (e.g., weathered bedrock, cavities, fractures), and evaluate ground material stiffness and bedrock topography near proposed wind turbine locations. Seismic data were acquired by Zonge International on August 5 through August 15, 2014. Rayleigh type surface waves were analyzed using the multichannel analysis of surface waves (MASW) and side scatter analysis (SSA) methods for a total of 44 seismic lines.

For each site, a two-dimensional (2-D) shear-wave velocity (V_s) profile was obtained using MASW for each of four lines. Average 1-D V_s profiles were calculated for each line to assist in the interpretation of the depth to bedrock and estimate the average velocity of subsurface layers. Pseudo three-dimensional (3-D) visualization of subsurface structure was achieved through the utilization of fence diagrams, a spatially accurate display of 2-D profiles plotted at their relative positions within the seismic grid. Approximate bedrock topography was mapped using an isovelocity surface rendered from the pseudo 3-D V_s volume. Probability density maps indicative of possible surface wave scatter locations were generated using SSA for depth ranges of 10-20 ft, 20-30 ft, and 30-50 ft.

The maximum investigation depth in the study area was typically 50-60 ft. In general, two distinct layers are interpreted on 2-D V_s profiles. The V_s of the shallow layer is less than 2000 ft/s, consistent with V_s expected for unconsolidated sediment, weathered or fractured limestone. Profiles transition to higher velocities indicative of more competent limestone at a depth of 10-30 ft, depending on the site. Average V_s of the limestone layer ranged from approximately 3000 ft/s at most sites to 5000 ft/s (at T11). Possible azimuthal shear-wave anisotropy was observed at sites T9, T10, and T11. The direction of maximum V_s is north-south, suggesting the possibility of increased stress parallel to this direction or aligned fractures with strike perpendicular to this direction. More detailed studies are required to precisely determine the direction of maximum V_s and cause of the anisotropy.

Localized zones of anomalously low V_s , anomalous horizontal or vertical change in V_s (e.g., velocity inversion), and/or high amplitude surface wave scatter are possible anomalies. A total of 36 possible anomalies are identified. Anomalies are generally interpreted as changes in material properties related to erosion/deposition, weathered bedrock surface, fractures, or karst-related features (e.g., cavity) depending upon the V_s characteristics of the anomaly, V_s structure on adjacent lines, and characteristics of surface wave scatter on probability density maps.

Introduction and Objectives

A wind turbine site requires a heavy loading across a relatively small area and must have a rock foundation capable of withstanding the dynamic vibration pattern generated by the rotating blades mounted at the top of a high tower. Safely supporting a tower base requires a potential site to have sufficiently high ground material stiffness down to several tens of feet below the top of bedrock (e.g., 50 feet). It is also essential that the rock be free of any anomalies that may compromise the overall stability of the tower foundation and the crane pad during construction. These anomalies include such features as cliff-faces or vertical fractures, uneven bedrock/weathered surface, a soft layer underlain by hard layer(s), voids of various sizes and origins, etc.

A proper site characterization therefore requires an investigation of the overall stiffness distribution beneath the area influencing tower stability. An equally important criterion is the effective detections of any anomalies. Seismically, stiffness of ground materials is directly linked to shear-wave velocity (V_s) of the material with a minor dependence on density. V_s is also an indicator sensitive to the presence of most of the aforementioned anomalies because of the significant contrast in stiffness as well as density. Surface waves are most often used to estimate the V_s structure of soil and bedrock (Miller et al., 1999; Stokoe et al., 1994) using the multi-channel analysis of surface waves (MASW) method (Park et al., 1999; Xia et al., 1999).

Surface waves are known to be sensitive to the presence of near-surface anomalies such as near-vertical fractures and voids. A significant amount of surface wave energy impinging against them is transformed into scattered surface waves due to anomalies acting as new sources of surface waves (Figure 1). Therefore, MASW data collected for V_s mapping can also be used to detect possible anomalies existing subsurface off the survey line using side-scattering analysis (SSA) of surface waves (Park and Miller, 2005).

Four lines of seismic data were acquired at each of eleven proposed wind turbine sites in St. Elizabeth Parish, Jamaica. Surface waves are analyzed to calculate shear-wave velocity (V_s), evaluate ground material stiffness and bedrock topography, and identify potential anomalies that might compromise the overall stability of the tower foundation (e.g., weathered bedrock surface, vertical fractures, voids, etc.). Final evaluation for the detection of possible anomalies is made through a composite interpretation of: 2-D V_s mapping, average 1-D V_s profiles, and pseudo 3-D V_s displays (fence diagrams) obtained from MASW; and probability density maps obtained from SSA.

Description of Methods

Multichannel Analysis of Surface Waves (MASW)

The propagation velocity (called phase velocity) of surface waves is frequency (or wavelength) dependent (this property is called dispersion). This dependency is determined mainly by the vertical V_s variation. By recording fundamental-mode Rayleigh type surface waves propagating horizontally and directly from the seismic source, the dispersion property can be measured and represented by a curve (called dispersion curve) depicting the variation of phase velocities with frequency. This curve is then used to back-calculate the vertical variation of V_s (called a 1-D V_s profile) through a process called inversion.

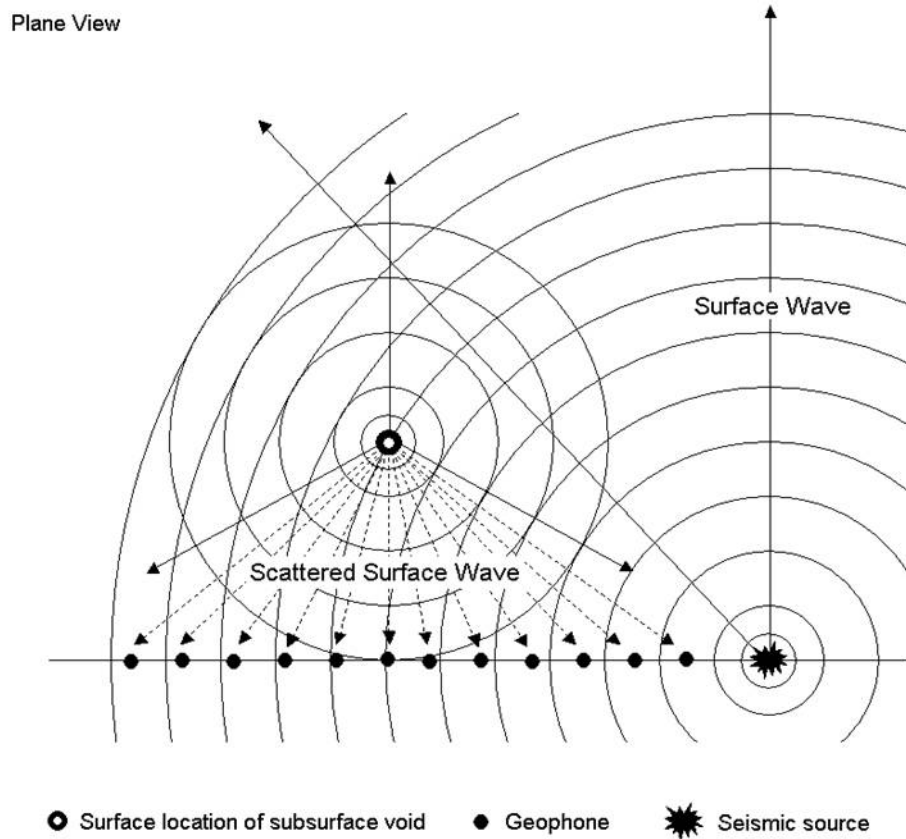


Figure 1. A plane-view schematic illustrating the scattered surface-wave generation that can be set off by a near-surface anomaly like a void.

The MASW method utilizes some of the pattern-recognition concepts provided by the multichannel recording and processing approaches. It employs multiple receivers (geophones) placed along a linear survey line with an equal spacing. Seismic waves generated by an impulsive source (e.g., sledgehammer) and propagating along the receiver line are recorded synchronously (Figure 2), enabling the recognition of various types of propagation characteristics.

Enhanced effectiveness in data processing allows one measurement with one source-receiver (SR) configuration to produce a 1-D Vs profile. By subsequently moving the same SR configuration along a preset survey line, multiple measurements can be made efficiently to produce a multiple number of 1-D Vs profiles which are then used to construct a 2-D Vs map (Figure 2). This 2-D Vs map represents a cross-sectional view of Vs distribution below the survey line. The bedrock topography is often identified by an interface where Vs rapidly increases (Miller et al., 1999) (Figure 3). Data collection over such multiple lines separated by a certain distance can lead to a pseudo 3-D Vs map that can depict the bedrock topography in 3-D mode (Miller et al., 1999). Large-scale anomalies can also be detected from unusually shaped Vs images through normal 2-D Vs mapping (Miller et al., 2000).

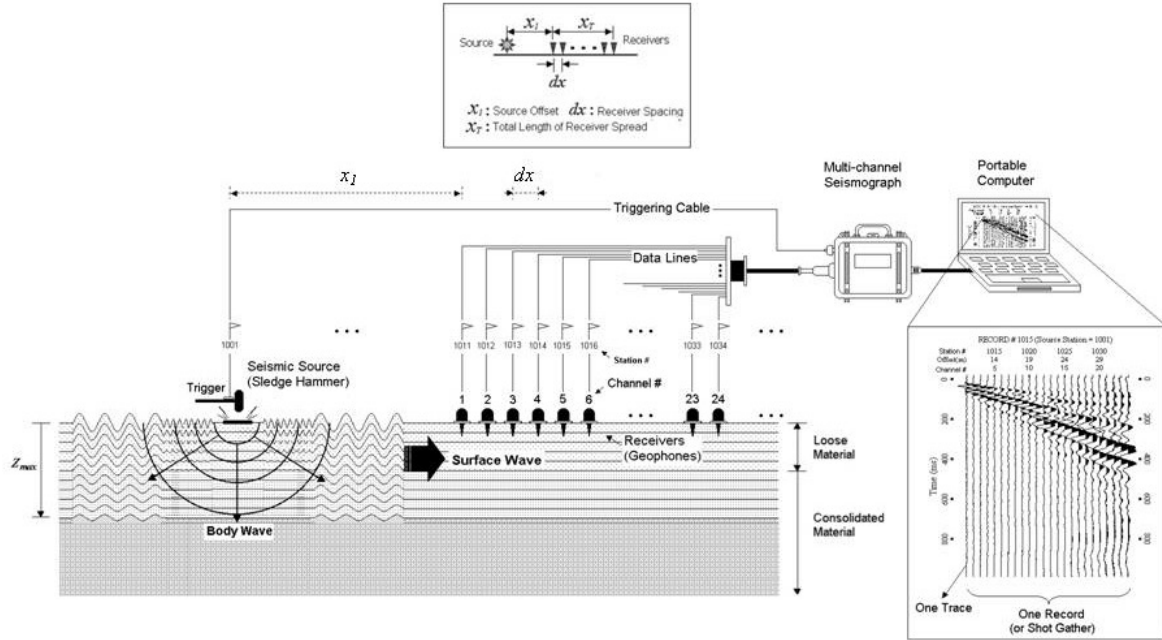


Figure 2. A schematic illustrating a typical field configuration with an MASW survey.

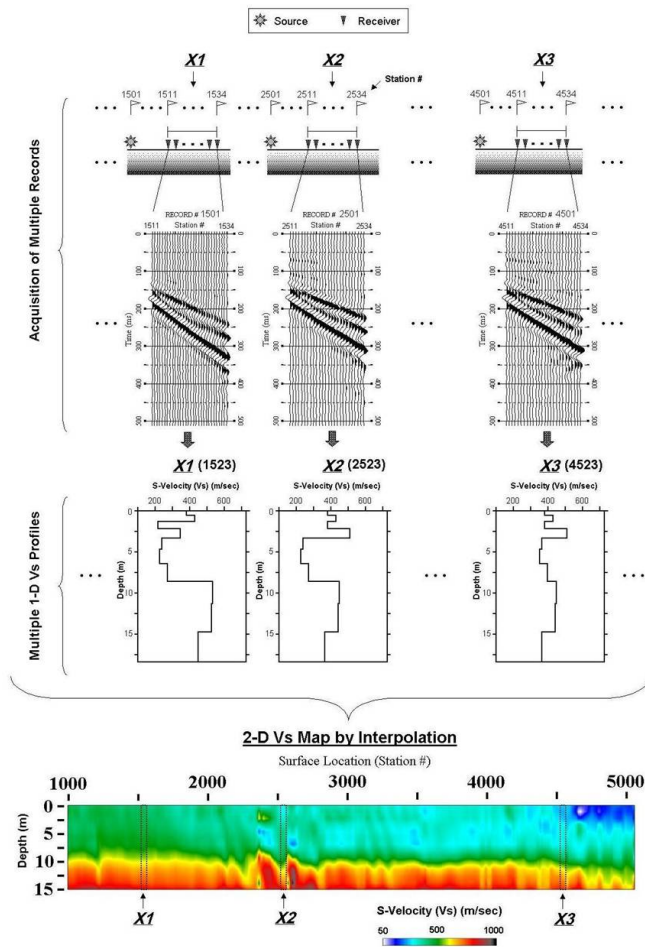


Figure 3. Illustration of the procedure used to generate a 2-D V_s map from a roll-along mode MASW survey.

Side Scatter Analysis (SSA)

According to Park and Miller (2005), when a void exists below surface location (x, y) , the scattered surface wave component of frequency f generated by impact of a source located at (x_s, y_s) and traveling with a phase velocity of $C(f)$ will reach a receiver at located at (x_r, y_r) at time $\delta t(f)$:

$$\delta t(f) = (L_1 + L_2)/C(f), \quad (1)$$

where

$$L_1 = \sqrt{(x_s - x)^2 + (y_s - y)^2}, \quad (2)$$

and

$$L_2 = \sqrt{(x_r - x)^2 + (y_r - y)^2}. \quad (3)$$

Each point (x, y) in a proposed grid is assumed to be a source of scattered surface waves (Figure 4). Selected traces that correspond to the proposed scattered wavefields are collapsed to their origin in time by applying a phase shift (equation 1) using the phase velocities $C(f)$ defined by a representative dispersion curve. Shifted traces stack coherently when an anomaly is present, focusing scattered surface wave energy to the anomaly location.

The collapsed waves are summed (stacked) to yield an indicator $P(x, y)$:

$$P(x, y) = \left| \sum_{traces} \sum_{f_1}^{f_2} e^{-j2\pi f \delta t(f)} R_{r,s}^{Norm}(jf) \right|, \quad (4)$$

where $R_{r,s}^{Norm}(jf)$ is the normalized Fourier transformation of the seismic trace recorded by the receiver at (x_r, y_r) when the seismic source was located at (x_s, y_s) . $P(x, y)$ is proportional to the intensity of scattering and, therefore, qualitatively the probability of the existence of an anomaly. When displayed in a 2-D format (probability density map), sources of surface wave scatter can be interpreted as areas with anomalous values of P . The depth range sensitive to this analysis is assumed to be half the range of wavelengths defined by the frequency range (f_1-f_2) used during processing:

$$z = \frac{\lambda}{2} = \frac{C(f)}{2f}, \quad (5)$$

where $C(f)$ is the corresponding surface wave phase velocity on the representative dispersion curve. Surface waves are sensitive to anomalies with diameters larger than $\sim 20\%$ of their depths.

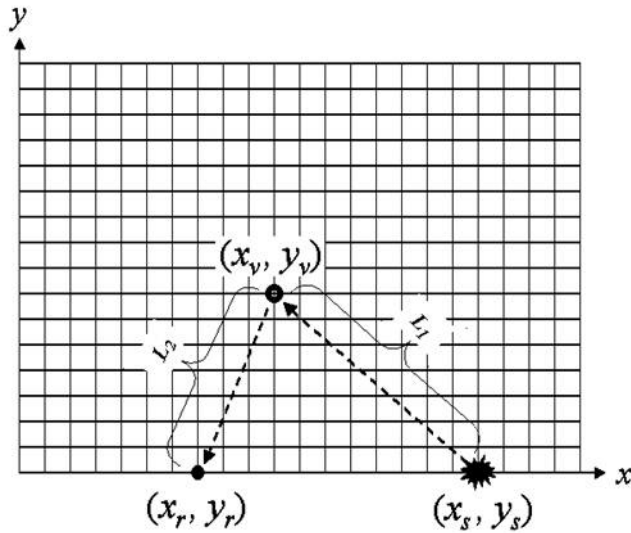


Figure 4. Each point in a proposed grid is assumed to be a possible source of scattered surface waves. Traces recorded by a receiver at (x_r, y_r) when the seismic source was located at (x_s, y_s) are focused to the origin (x, y) .

Geologic Setting

The study area is located in the Santa Cruz Mountains in St. Elizabeth Parish, Jamaica. Bedrock is the White Limestone Group (Mitchell, 2013), which formed during the Late Oligocene to Early Miocene across a shallow-water platform (Robinson, 1994). Several known faults oriented predominately northwest-southeast and northeast-southwest exist near the study area (Porter et al, 1974). According to prior geotechnical investigations at this site, the limestone is shallow, fractured with possible solution cavities, and is overlain by layer of silty clay, sand, and/or gravel at some locations (Hay, 2014).

Data Acquisition and Processing

Four lines of seismic data were acquired by Zonge International at each of eleven sites (Figure 5, Table 1). A configuration of three parallel lines separated by 48 ft and one perpendicular line was centered on the proposed wind turbine location (Figure 6). Each fixed spread of receivers consisted of 48 4.5 Hz vertical geophones separated by 4 ft. The seismic source was a sledgehammer. For each line, the initial source station was located 16 ft off end from the spread of receivers. The source moved at 4 ft intervals to the center of the spread for lines 1 and 3, and through to the end of the spread for lines 2 and 4. Multiple records were acquired and recorded separately at each source location. Dead or noisy traces were muted, and records acquired at the same shot station were vertically stacked during processing to minimize ambient noise and increase the signal-to-noise ratio.

Shot gathers were analyzed using SurfSeis, a proprietary software package from the Kansas Geological Survey. At each site, representative shot gathers were selected from each line to test for offset and spread length that produced phase velocity versus frequency plots (overtone images) with optimum resolution of fundamental mode Rayleigh wave energy (Figure 7). Selected traces were cut from the fixed spread shot gathers to simulate rolling acquisition with the optimum offset and spread length. An overtone image was generated for each shot gather and the fundamental mode dispersion curve was picked. Each dispersion curve was inverted (Xia et al., 1999) to obtain a 1-D Vs profile, which was assigned to the surface location at the

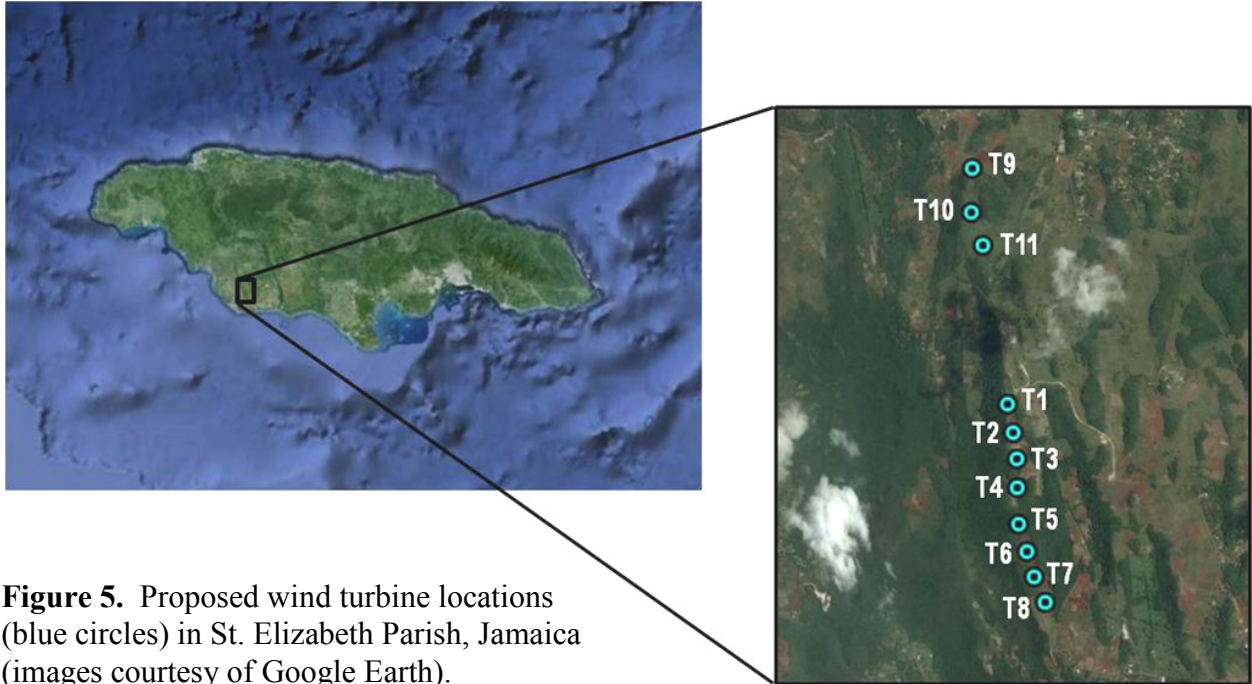


Figure 5. Proposed wind turbine locations (blue circles) in St. Elizabeth Parish, Jamaica (images courtesy of Google Earth).

Table 1. Coordinates of proposed wind turbine locations and azimuths of line 1 at each site (0° = north).

tower	latitude	longitude	line 1 azimuth (°)	line 2-4 azimuth (°)
T1*	17.93992	-77.69798	75	345
T2	17.93840	-77.69766	90	0
T3	17.93700	-77.69745	0	90
T4	17.93547	-77.69743	0	90
T5	17.93354	-77.69735	90	0
T6	17.93211	-77.69689	305	35
T7	17.93080	-77.69649	305	35
T8	17.92950	-77.69588	0	90
T9	17.95245	-77.69994	90	0
T10	17.95015	-77.70000	355	85
T11	17.94838	-77.69935	0	90

*T1 was moved 10 m east of the original surveyed location during seismic acquisition due to topography. T1 coordinates listed here were calculated from the surveyed coordinates.

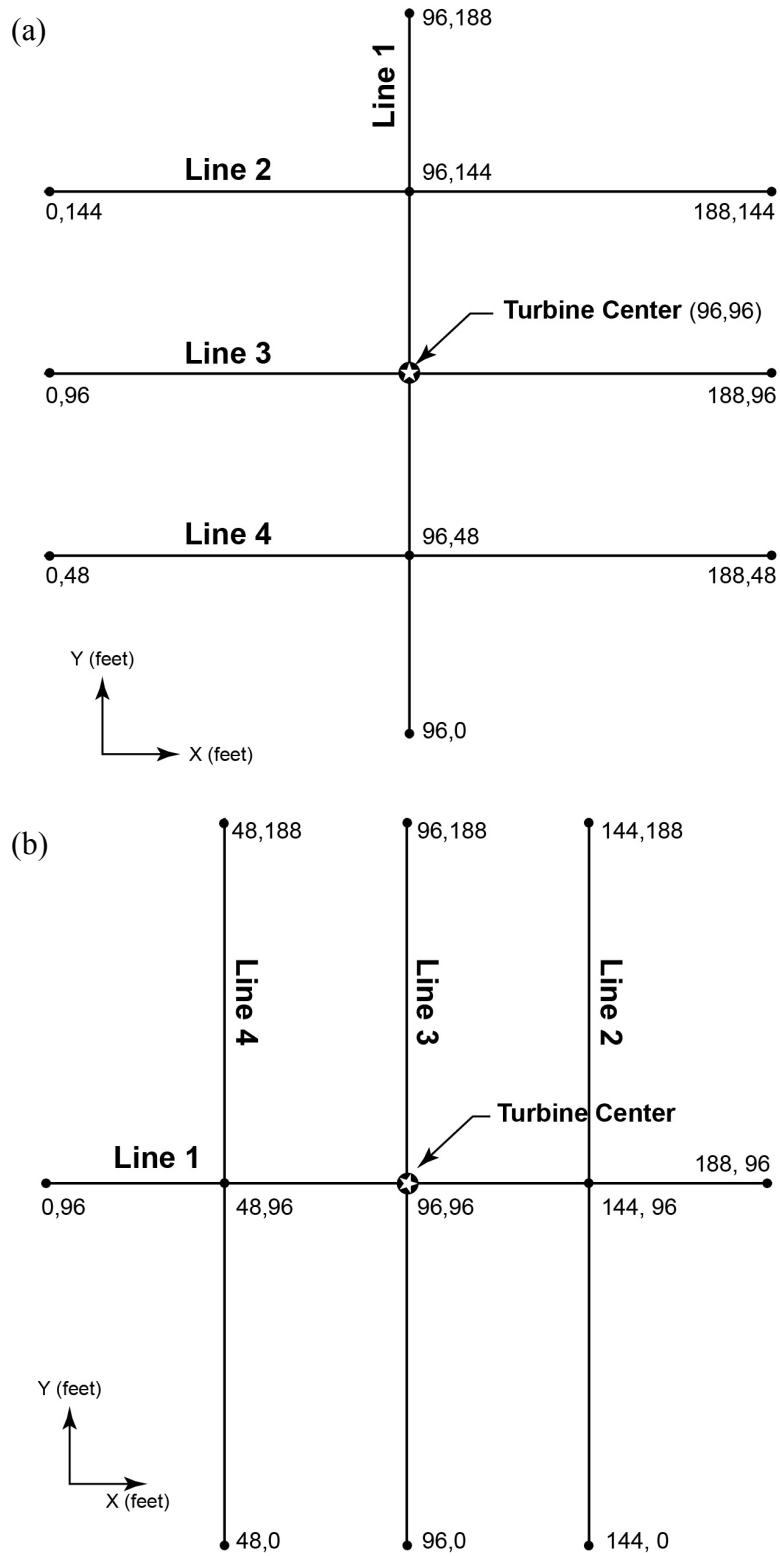


Figure 6. Configuration of four seismic lines centered on the proposed wind turbine location for (a) sites T3, T4, T6, T7, T8, T10 and T11, and (b) T1, T2, T5 and T9.

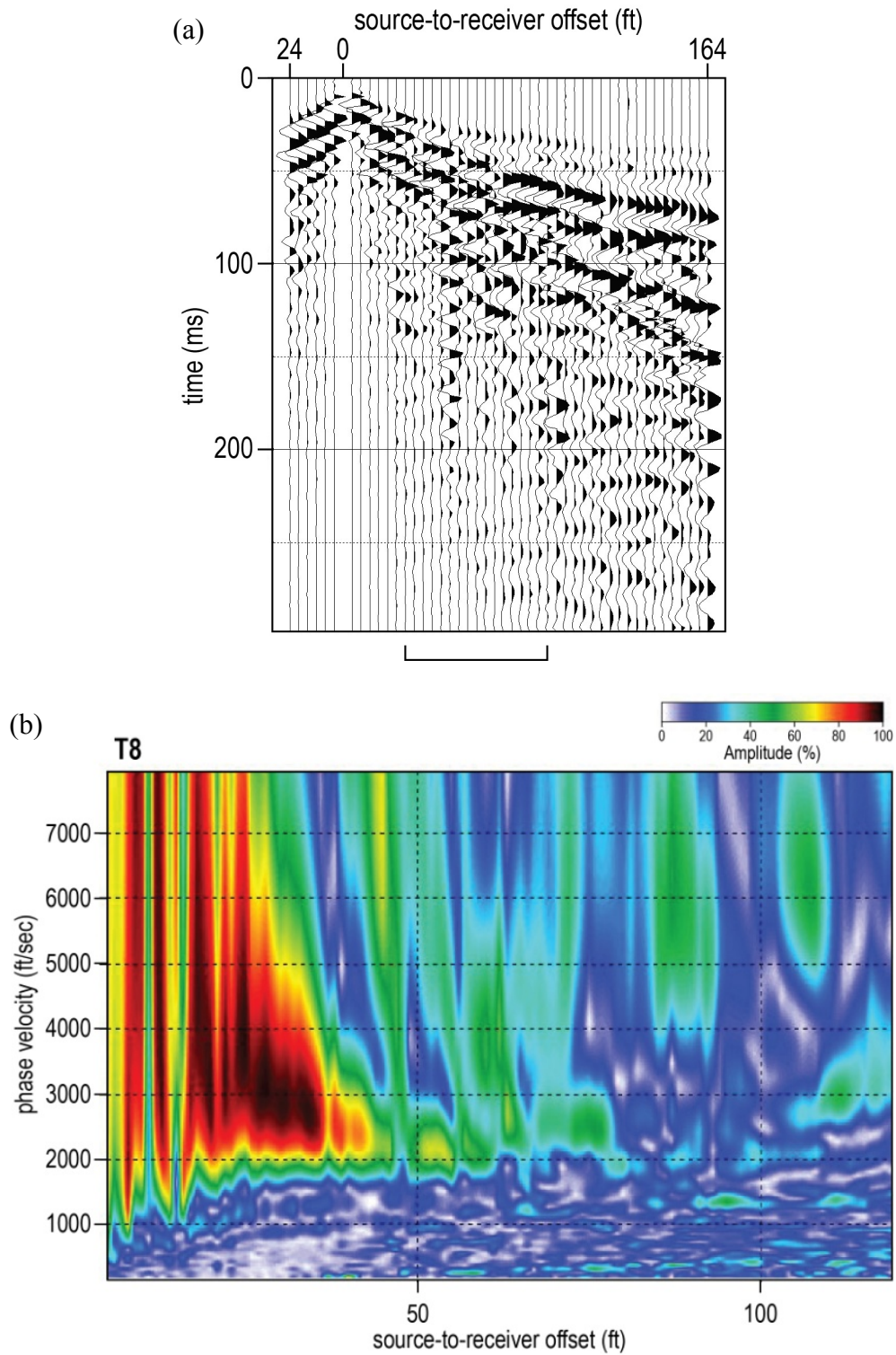


Figure 7. (a) Representative shot record and (b) resulting overtone image from seismic data acquired at T8.

center of the spread used in the analysis. For each line, 1-D Vs profiles were assembled in a 2-D cross-sectional format to produce a 2-D Vs profile.

The statistical mean of 1-D profiles was calculated to determine the average 1-D Vs profile of each line. Pseudo 3-D Vs volumes (fence diagrams) were generated using Voxler, a commercial 3-D visualization package by Golden Software. Each 2-D Vs profile was plotted at the spatial location of the line from which it was calculated with respect to the four-line grid. Shear-wave velocities were interpolated and/or extrapolated to render a 3-D Vs volume. The approximate bedrock topography was mapped using the isovelocity surface defined by the top of bedrock Vs interpreted from the average 1-D Vs profiles.

Side scatter analysis was performed using SeisUtilities, a proprietary software package from the Kansas Geological Survey. An $f-k$ filter was applied to shot gathers from lines 1 and 2 to attenuate the primary surface wave energy and enhance the scattered surface wave signal. The dominant dispersion pattern was picked on an overtone image that is representative of the site. For each surface location in the (x, y) grid defined by lines 2 and 4, a frequency-dependent phase shift (equation 1) was applied to traces on shot gathers assuming a scattered surface waves originated from that location. Probability density maps were generated by summing the amplitude of the focused surface wave signal within the frequency ranges that corresponds to depths of 10-20 ft, 20-30 ft, and 30-50 ft (equation 4).

Upon completion and review of preliminary results, some lines were reprocessed using advanced filtering techniques and processing parameters tuned for optimum extraction of the fundamental mode dispersion pattern.

Results

A summary of locations of possible anomalies is given in Table 2. *Note:* The convention for the direction of the x and y axes with respect to the grid of seismic lines was not consistent across all sites. Interpreted anomalies did not change, but anomaly locations were updated for the coordinate system defined by the reversed grid (Figure 6b) used at sites T1, T2, T5, and T9. Results of final processing are located in the following appendices:

- Appendix A: Final 2-D Vs profiles obtained using MASW
- Appendix B: Probability density maps obtained using SSA
- Appendix C: Average 1-D Vs profiles
- Appendix D: Vs fence diagrams
- Appendix E: Isovelocity surfaces
- Appendix F: Potential anomaly locations superimposed on field layout diagrams

Isovelocity surfaces are viewed from the corner of the site perimeter where the line 1 starts at the bottom left and ends at the top right (Figure 8a). Fence diagrams are viewed both from the same corner as the isovelocity surfaces, and from the opposite corner of the site perimeter where line 1 starts at the top right and ends at the bottom left (Figure 8b).

Table 2. Locations of potential anomalies given in (x,y) coordinates, as defined in the field layout diagrams (Figure 6).

site	anomaly 1	anomaly 2	anomaly 3	anomaly 4	anomaly 5
T1†	(48,52)	-	-	-	-
T2†	(96,64)	-	-	-	-
T3	(96,66)	(76,96)	(112,144)	-	-
T4*	(128,96)	(120,130)	-	-	-
T5†	(48,60)	(124,96)	(96,72)	-	-
T6	(96,92)	(120,96)	(52,110)	(96,132)	-
T7	(100,96)	(92,144)	(150,110)	(118,48)	-
T8*	(92,96)	(120,96)	(96,78)	(24,85)	(64,96)
T9†	(86,96)	(54,96)	(96,112)	(96,56)	-
T10	(96,90)	(80,96)	(88,48)	(52,100)	-
T11*	(96,100)	(128,48)	(0,70)	(72,144)	-

*Anomalies were modified based on the results of final processing.

†Interpreted anomalies did not change, but anomaly locations were updated for the coordinate system defined by the reversed grid (Figure 6b).

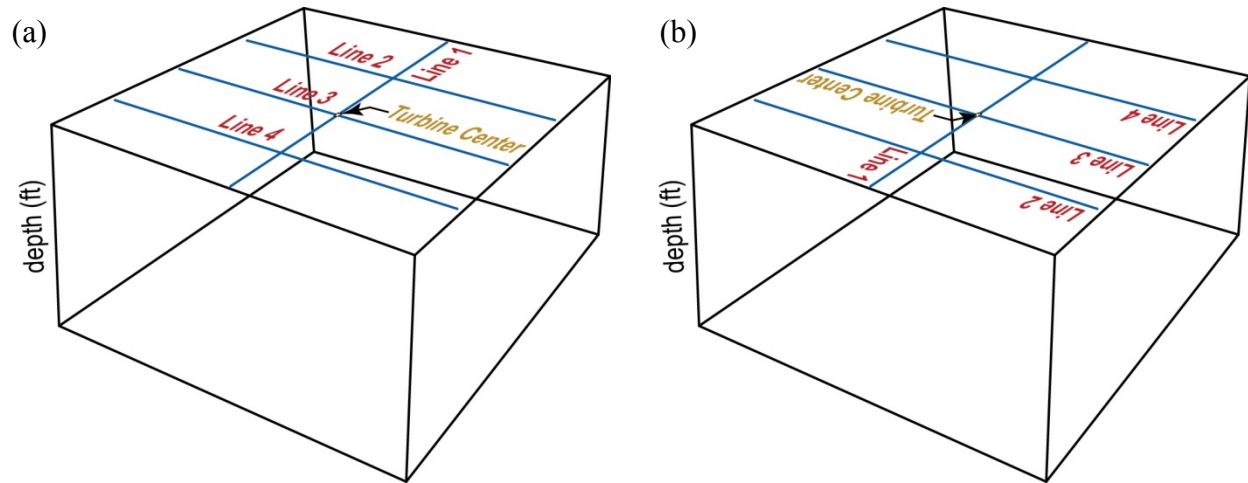


Figure 8. Diagrams illustrating the perspective used to display (a) isovelocity surfaces and fence diagrams, and (b) fence diagrams from the view at the opposite corner of the site perimeter.

Discussion

The maximum investigation depth in the study area was typically 50-60 ft. In general, two distinct layers are interpreted on 2-D Vs profiles. The Vs of the shallow layer is less than 2000 ft/s, consistent with Vs expected for unconsolidated sediment, weathered or fractured limestone. Profiles transition to higher velocities indicative of more competent limestone at a depth of 10-30 ft, depending on the site. Average Vs of the limestone layer ranged from approximately 3000 ft/s at most sites to 5000 ft/s (at T11). Possible azimuthal shear-wave anisotropy was observed at sites T9, T10, and T11. Causes of anisotropy include aligned fractures and unequal horizontal stresses (Lynn and Thompsen, 1990). The direction of maximum Vs is approximately north-south, suggesting the possibility of increased stress in this direction or aligned fractures oriented perpendicular to this direction (DeVault et al., 2002). More detailed studies are required to precisely determine the direction of maximum Vs and cause of the anisotropy.

Localized zones of anomalously low Vs, anomalous horizontal or vertical change in Vs (e.g., velocity inversion), and/or high amplitude surface wave scatter are possible anomalies. Confidence is greater when the anomaly is consistent across multiple analyses (e.g., SSA and MASW, multiple MASW lines, etc.). A total of 36 possible anomalies were identified. Anomalies are generally interpreted as changes in material properties related to erosion/deposition, weathered bedrock surface, fractures, or karst-related features (e.g., cavity) depending upon the Vs characteristics of the anomaly, Vs structure on adjacent lines, and characteristics of surface wave scatter on probability density maps.

T1

The shear-wave velocity from the surface to approximately 20 ft is less than 2000 ft/s, consistent with the velocity expected for weathered or fractured limestone. Beneath 20 ft, the velocity is 3000-4500 ft/s, consistent with the velocity expected for more competent limestone bedrock. Horizontal velocity variability in the limestone bedrock may be related to deposition or erosion. Anomaly 1 is low bedrock velocity from stations $y = 46-92$ ft on line 4 (Figure A-1d) relative to other lines at site T1. This velocity is consistent with bedrock velocity at other sites in the study area and, therefore, may be a depositional feature. However, SSA results are indicative of surface wave scatter near this location at a depth of 30-50 ft that extends from line 4 through at least line 3 (Figure B-1c). Surface wave scatter may originate from a change in bedrock topography due to variability in weathering or possible fracture.

T2

The shear-wave velocity from the surface to 15-20 ft is approximately 1200 ft/s, consistent with the velocity expected for unconsolidated sediment, weathered or fractured limestone. Below 20 ft is more competent limestone bedrock with a velocity of 2500-3500 ft/s. A very subtle velocity inversion in the limestone bedrock at ~35 ft is most likely related to deposition. Anomaly 1 is an anomalously high velocity in the upper 20 ft from $y = 32-72$ ft on line 3 (Figure A-2c). This most likely represents deposition of a stiffer material over looser material. This is consistent with surface wave scatter at the boundary between the two materials at a depth of 10-20 ft (Figure B-2a).

T3

The shear-wave velocity from the surface to 15 ft is approximately 1500 ft/s, consistent with the velocity expected for unconsolidated sediment, weathered or fractured limestone. The highest picked frequency on dispersion curves at this site corresponds to a depth of approximately 10 ft. Therefore, the high velocity layer at 5-10 ft (Figure A-3) is low confidence. The average velocity beneath 15 ft is approximately 3500 ft/s, which is indicative of more competent limestone bedrock.

Anomaly 1 is a localized zone of low velocity at a depth of 20-40 ft from $y = 64$ -80 ft on line 1 (Figure A-3a). The velocity in this zone is approximately 50% less than at adjacent stations. There is a subtle anomaly near this location on the probability density map (Figure B-3b), suggesting it may be a karst-related cavity.

Anomaly 2 is a low velocity zone in the limestone bedrock at a depth of 20-30 ft from $x = 66$ -88 ft on line 3 (Figure A-3c). This may be related to a horizontal decrease in V_s at $x = 64$ ft on line 4 (Figure A-3b) and $x = 72$ -92 ft on line 2 (Figure A-3c), suggesting the possibility of a fracture. This interpretation is supported by scattered surface wave energy near these locations at a depth of approximately 10-20 ft (Figure B-3a).

Anomaly 3 is a decrease in bedrock velocity and increase in depth to bedrock at $x = 96$ -148 ft on line 2 (Figure A-3b). Because there is no decrease in velocity at this location on lines 3 or 4, this is likely a local depositional or erosional feature. A decrease in V_s and increase in the depth to bedrock on line 1 at the line 2 crossing is consistent with the observations from line 2 (Figure D-3). The isovelocity surface suggests a change in bedrock topography at the northeast corner of the study area (Figure E-3).

T4

The fundamental mode dispersion pattern on line 1 had significant higher mode interference. Because fundamental mode energy is indistinguishable from higher mode energy on this line, dispersion curve picking followed the dominant (higher mode) trend. Although these velocities are not representative of the shear-wave velocity of the subsurface materials (and, therefore, do not match the line 3 and 4 V_s where they intersect line 1, Figure B-4), the resulting 2-D V_s profile is likely representative of the general velocity trend and geologic structure. Higher mode interference is least on lines 2 and 3 and, therefore, V_s on these lines has the least uncertainty.

The shear-wave velocity from the surface to 10-15 ft is approximately 1000 ft/s, consistent with the velocity expected for unconsolidated sediment or weathered limestone. The shear-wave velocity below 10-15 ft is 2000-4500 ft/s, which is indicative of more competent limestone bedrock. A subtle velocity inversion at a depth of 20-25 ft is likely related to deposition of the limestone. The isovelocity surface (Figure E-4) suggests an increase in bedrock elevation between lines 3 and 4. An increase in V_s on line 1 near the line 4 crossing (Figure A-4a) is consistent with this interpretation. Uncertainty in V_s on line 4 is greater than on lines 2 and 3 (due to higher mode interference); therefore, the change in bedrock topography may be less dramatic than the isovelocity surface suggests.

Anomaly 1 is a lateral decrease in bedrock velocity at approximately $x = 120$ ft on line 3 (Figure A-4c). Linear scattered surface wave energy at all depths at this location suggests the possibility of a N-S oriented fracture (Figure B-4). There are only subtle changes in V_s at this location on adjacent lines (Figures A-4b and A-4d) and, therefore, this anomaly might instead be related to variable weathering of the limestone bedrock and change in bedrock topography.

Anomaly 2 is a surface wave scatter at a depth of 30-50 ft near line 2 (Figure B-4c). This is consistent with a change in the dispersion pattern on overtone images and a subtle decrease in V_s from $x = 104-118$ ft on line 2 (Figure A-4b), and may be indicative of a small cavity.

T5

The shear-wave velocity from the surface to 15-20 ft is less than 2000 ft/s, consistent with the velocity expected for weathered or fractured limestone. Beneath 15-20 ft, the shear-wave velocity is 3000-5000 ft/s, which suggests more competent limestone. Dispersion patterns on line 1 suggest that the general trend of velocity decreasing from west to east is most likely accurate. The velocity structure on lines 2-4 supports this observation. Higher mode surface waves at site T5 have higher amplitudes and greater interference with the fundamental mode relative to other sites in the study area. In general, uncertainty in the fundamental mode dispersion curve, and thus V_s , is greater at this site due to low signal-to-noise ratio.

Anomaly 1 is a low velocity zone at ~40 ft near the edge of the study area centered at station $y = 56-72$ ft on line 4 (Figure A-5d). Dispersion patterns at this location are inversely dispersive, indicative of velocity decreasing with depth. A possible scatter at 30-50 ft (Figure B-5c) near this location suggests the anomaly may be caused by a karst-related feature. However, the surface wave scatter is relatively low amplitude and, therefore, confidence in this anomaly is moderate.

Anomaly 2 is a low velocity zone in the limestone at 60 ft near $x = 124$ ft on line 1 (Figure A-5a). There is no corresponding surface wave scatter at this location (Figure B-5). Therefore, the velocity decrease may be related to depositional/erosional variability. The 45% velocity decrease (relative to adjacent stations) may not be representative of changes in material stiffness, but may be in part related to instability of the inversion algorithm.

Anomaly 3 is a low velocity zone at 40-70 ft depth from $y = 66-88$ ft on line 3 (Figure A-5c). This anomaly has a similar velocity structure and is located adjacent to anomaly 1, suggesting they could be related. However, there is no corresponding surface wave scatter at the location of anomaly 3 (Figure B-5). This anomaly may be related to uncertainty in the fundamental mode dispersion pattern and instability of the inversion algorithm.

T6

Three distinct layers can be interpreted on the 2-D V_s profiles from site T6 (Figure A-6). The shear-wave velocity from the surface to 20 ft depth is approximately 1000 ft/s, consistent with the velocity expected for unconsolidated sediment or weathered limestone. The shear-wave velocity from 20-40 ft is approximately 2000 ft/s on average, indicative of weathered or fractured limestone. Below 40 ft is a relatively large velocity gradient with V_s exceeding 3500 ft/s, indicating the limestone at this depth is more competent.

Anomaly 1 is an area of particularly low velocity in the unconsolidated or weathered layer from $y = 80-98$ ft and may be suggestive of fill type material near the proposed turbine center (Figure A-6a). It is consistent with low velocity at this depth on line 3 where it intersects line 1 (Figure A-6c). There is no corresponding surface wave scatter, which suggests the stiffness of this material may not be dramatically different than stiffness of the surrounding sediment.

Anomaly 2 is a low velocity zone at 20-40 ft from $x = 108-124$ ft on line 3 that may represent a cavity (Figure A-6c). Reduced velocity at 20-25 ft indicates possible slumping of the overlying layer.

Anomaly 3 is a high confidence localized zone of low velocity at 40 ft overlain by a high velocity “halo” at a depth of 25-30 ft from $x = 48-56$ ft on line 3 (Figure A-6c). This is suggestive of a void with stress building in the roof rock. A prominent surface wave scatter near this location (Figure B-6b and B-6c) supports this interpretation.

Anomaly 4 is an abrupt decrease in the shear-wave velocity of the limestone near station $y = 128$ ft on line 1 (Figure A-6a). Surface wave scatter at a depth of 30-50 ft near this location (Figure B-6b) suggests this anomaly may be a cavity or fracture.

T7

The shear-wave velocity from the surface to 10 ft is less than 1000 ft/s, consistent with the velocity expected for unconsolidated sediment, weathered or fractured limestone. The shear-wave velocity below 10 ft is approximately 2500 ft/s on average, indicative of weathered and/or fractured limestone. Velocity variability in the layers above 40 ft suggests variability in deposition/erosion or karst-related features.

Anomaly 1 is a localized zone of low velocity located at a depth of approximately 25 ft from $x = 96-100$ ft on line 3 (Figure A-7c). The velocity is approximately 40% slower than at adjacent stations and be indicative of a solution cavity or deposition of stiffer material over looser, possibly fill type material near the proposed turbine center. This feature is consistent with a low-velocity zone imaged at the same depth on line 1 where it intersects line 3 (Figure A-7a) and surface wave scatter near this location at a depth of 10-20 ft (Figure B-7a) and is, therefore, high confidence.

Anomaly 2 is a low velocity zone in the limestone below 20 ft from $x = 96-136$ ft on line 2 (Figure A-7b). It may be related to natural variability in the limestone deposition. However, this zone is consistent with moderate amplitude surface wave scatter (Figure B-7b), suggesting the possibility of a fracture or karst-related feature.

High amplitude surface wave scatter is observed from 20-50 ft along the northeast boundary of the study area, extending southwest possibly as far as line 1 (Figures B-7b and B-7c). Anomaly 3 is a prominent surface wave scatter at a depth of 20-30 ft (Figure B-7b). Without velocity information at this location, it is difficult to interpret the origin of this scatter zone. Changes in material stiffness, variability in the bedrock surface, karst or fracture(s) are all possible sources of surface wave scatter.

Anomaly 4 is a decrease in velocity of the limestone at a depth of ~ 30 ft from $x = 112-128$ ft on line 4 (Figure A-7d). The decrease in velocity is approximately 35-40% relative to adjacent stations. Variability of the limestone velocity may be related to deposition or erosion. However, this anomaly may be related to the surface wave scatter observed on the northeast portion of the study area, suggesting it may be a karst-related feature (anomaly 3).

Anomaly 5 is a zone of lower velocity (relative to the remainder of the line) from $x = 40-84$ ft on line 4 (Figure A-7d). Because there is no corresponding surface wave scatter in this zone and the velocity is consistent with the limestone velocity on the other lines at this site, it is likely related to variability in deposition of the limestone.

T8

The signal-to-noise ratio of the fundamental mode Rayleigh wave is lower on lines 2 and 3 relative to lines 1 and 4. Enhanced processing techniques were applied to lines 2 and 3 to identify the fundamental mode dispersion pattern with greater confidence. The 2-D Vs profiles

resulting from the re-picked dispersion curves have less uncertainty than the preliminary profiles, and are more consistent with the velocities and geologic structure observed on lines 1 and 4.

The shear-wave velocity from the surface to ~20 ft is less than 2000 ft/s, consistent with the velocity expected for weathered or fractured limestone. The shear-wave velocity below 20 ft is 3000 ft/s on average, indicative of more competent limestone. Based on the 2-D Vs profiles of lines 2-4, Vs appears to increase to the north (Figure A-8). Shear-wave velocities on line 1 are consistent with this observation. This may be related to increase in local stress to the north or natural variation in deposition of the limestone.

Anomalies 1, 2, and 3 were identified as separate anomalies based on the preliminary 2-D Vs profiles. Reprocessed 2-D Vs profiles (Figures A-8 and D-8) suggest that these anomalies may in fact be related to the same structure. A zone of low velocity located at a depth ~50 ft extends from $y = 66-108$ ft on line 1 (Figure A-8a) and $x = 76-128$ ft on line 3 (Figure A-8c). The absence of a prominent surface wave scatter and lack of similar horizontal Vs discontinuity on lines 2 and 4 suggest this anomaly is most likely not a fracture, and may represent solution altered limestone.

Anomaly 4 is a surface wave scatter along the western boundary of the site at a depth of approximately 20-50 ft (Figures B-8b and 8c). Without velocity information at this location, it is difficult to interpret the origin of this scatter. Changes in material stiffness, variability in the bedrock surface, karst or fracture(s) are all possible sources of surface wave scatter.

Anomaly 5 is a localized low velocity zone at ~40 ft from $x = 60-68$ ft on line 3 (Figure A-8c). The dispersion pattern observed on overtone images from this location is consistent with the dispersion pattern expected for a velocity decrease at this depth. Low amplitude surface wave scatter near this location (Figure B-8c) suggests a possible cavity. The signal-to-noise ratio of the fundamental mode Rayleigh wave is relatively low due to higher mode interference and, therefore, confidence in this anomaly is low to moderate.

T9

The shear-wave velocity from the surface to ~15 ft depth is approximately 1000 ft/s, consistent with the velocity expected for unconsolidated material, weathered or fractured limestone. The shear-wave velocity beneath ~15 ft ranges from 2000-3400 ft/s, which is indicative of limestone that may be weathered or fractured in some places. In general, from line 2 to line 4 the thickness and horizontal extent of the shallow unconsolidated layer decreases and Vs increases. This suggests that the limestone is closer to the surface on the western perimeter of the site (Figure E-9). Shear-wave velocities on lines 2-4 are slightly higher than on line 1 (Figure A-9), suggesting azimuthal shear-wave velocity anisotropy with the direction of maximum Vs approximately north-south.

Anomaly 1 is a particularly low velocity within the unconsolidated layer at $x = 76-88$ ft on line 1 (Figure A-9a) and may be suggestive of fill material near the proposed turbine center. It is consistent with the low velocity at this depth on line 3 where it intersects line 1 (Figure A-9c).

Anomaly 2 is a low velocity zone at a depth of ~30 ft from $x = 44-70$ ft on line 1 (Figure A-9a). This anomaly is suggestive of erosional/depositional variability and/or karst-related features. Although Vs on line 4 at the line 1 intersection is not identical (at least in part due to anisotropy), it is suggestive of a velocity inversion at this location (Figure A-9d), which supports the existence of this anomaly.

Anomaly 3 is a low velocity zone at a depth of 20-40 ft from $y = 104-118$ ft on line 3 (Figure A-9c). Surface wave scatter at a depth of 30-50 ft near this location is suggestive of a possible karst-related feature near the proposed turbine center.

Anomaly 4 is a localized area of low velocity at a depth of 30-40 ft at $y = 56-58$ ft on line 3 (Figure A-9c). The dispersion pattern on the overtone image from this station is consistent with the pattern expected for a void at this depth. However, lack of strong surface wave scatter near this location suggests it may be a result of instability in the inversion algorithm and, therefore, confidence in this anomaly is low relative to other anomalies at this site.

T10

The shear-wave velocity from the surface to 10-20 ft depth is approximately 1000 ft/s, consistent with the velocity expected for unconsolidated sediment or weathered limestone. The shear-wave velocity below 20 ft is approximately 2000 ft/s on average, which is low for competent limestone and may be indicative of fractured limestone. Velocity variability in the limestone suggests karst-related features. In general, V_s on line 1 is slightly higher than lines 2-4, suggesting azimuthal shear-wave velocity anisotropy with the direction of maximum V_s approximately north-south. This is consistent with the possible anisotropy observed at site T9.

Anomaly 1 is a small zone of low velocity at a depth of 40-50 ft at $y = 84-92$ ft on line 1 (Figure A-10a), and may be indicative of a cavity near the proposed turbine center. Dispersion patterns near this location are consistent with the dispersion pattern expected for a decrease in velocity at this depth. Therefore, confidence in this anomaly is high.

Anomalies 2 and 3 are relatively high confidence areas of low velocity from 20-60 ft from $x = 66-96$ ft on line 3 (Figure A-10c) and $x = 70-108$ ft on line 4 (Figure A-10d). These may be karst-related features that might have connectivity with one another, and possibly with anomaly 1.

Anomaly 4 is surface wave scatter at a depth of 20-30 ft (Figure B-10b). This is consistent with a 5-10 ft thick low velocity layer at a depth of approximately 20 ft from $x = 52-80$ ft on lines 2 (Figure A-10b) and $x = 44-72$ ft on line 3 (Figure A-10c), which may be indicative of deposition of stiffer material over loose, unconsolidated material.

T11

The signal-to-noise ratio of the fundamental mode energy on overtone images is low on line 3 relative to the other lines at site T11. Dispersion curves on this line were re-picked to avoid dispersion variability related to noise and, where data quality allows, lower frequencies were picked to extend the depth of investigation to below 40 ft. The final picked dispersion curves follow a smoother trend that more accurately represents the true dispersion pattern of the fundamental mode. Confidence is higher in the resulting 2-D V_s profile, and consistent with the V_s observed on other lines at this site.

High amplitude surface wave scatter is observed on the western boundary of the site on the preliminary probability density maps (Figure B-11). Additional scatter in the center of the site is low amplitude, relative to the scatter on the western boundary and, therefore, difficult to interpret. Because the velocity structure and thus dispersion pattern varies, one dispersion pattern may not be representative of the entire site. Therefore, side scatter analysis was repeated using a dispersion curve that was more representative of the central and eastern areas of the site, enhancing surface wave scatter in these regions (Figure B-12). The scatter on the western edge was still very strong. To increase the amplitude of scatter within the central and eastern portions

of the site, the display of the reprocessed results is limited to locations east of $x = 20$. Both SSA results are complementary and, together, represent surface wave scatter at site T11.

Shear-wave velocity profiles indicate no unconsolidated layer consistent across the site within the depths of investigation, suggesting that the limestone bedrock is at or near the surface (less than 5 ft). Therefore, the bedrock surface is approximately equivalent to surface topography. To delineate features beneath the bedrock surface, a faster velocity was selected to define the isovelocity surface at this site (Figure E-11).

Shear-wave velocities at site T11 are faster than the other sites in the study area. Limestone velocities range from approximately 2000-7000 ft/s (Figure A-11). In general, V_s on line 1 is slightly higher than lines 2-4, suggesting there may be azimuthal shear-wave velocity anisotropy, with the direction of maximum V_s approximately north-south. This is consistent with the possible anisotropy observed at sites T9 and T10. The 2-D V_s structure is irregular with alternating low and high velocity, both vertically and horizontally. This may be in part related to natural variability in deposition or cementation; however, the variability of dispersion patterns and surface wave scatter throughout the site suggest there may be fractures and/or karst-related features.

Anomaly 1 is an area of low velocity at a depth of ~ 40 ft from $y = 72-104$ ft on line 1 (Figure A-11a). This is consistent with the velocity profile on line 3 at the line 1 crossing (Figure A-11c) and may suggest a karst-related feature near the proposed turbine center. The isovelocity surface suggests a possible cavity or solution altering near the location of this anomaly (Figure E-11b). This area is also consistent with linear surface wave scatter that extends from east of the center of line 4 toward the west end of line 2 (Figure B-12a), suggesting the possibility of a fracture near this location.

Anomaly 2 is an area from $x = 108-128$ ft on line 4 with a Lamb wave dispersion pattern. This pattern suggests a shallow velocity inversion. The velocities at approximately 5-15 ft and 40-50 ft are some of the slowest at this site (Figure A-11d), suggesting weathered or fractured limestone and/or karst-related features.

Anomaly 3 is a high amplitude shallow scatter near the western edge of the study area (Figure B-11a). Without velocity information at this location, it is difficult to interpret the origin of this scatter. Changes in material stiffness, variability in the bedrock surface, karst or fracture(s) are all possible sources of surface wave scatter.

Anomaly 4 is a localized low velocity zone at ~ 40 ft from $x = 68-76$ ft on line 2 (Figure A-11b), which may be indicative of a karst-related feature.

References

- DeVault, B., T.L. Davis, I. Tsvankin, R. Verm, and F. Hilterman, 2002, Multicomponent AVO analysis, Vacuum Field, New Mexico: *Geophysics*, v. 67, p. 701-710.
- Hay, C., 2014, Soil Investigation Draft Report: NHL Engineering Limited, 134 p.
- Lynn, H.B., and L.A. Thompsen, 1990, Reflection shear-wave data collected near the principle axes of azimuthal anisotropy: *Geophysics*, v. 55, p. 147-156.
- Miller, R.D., C.B. Park, J.M. Ivanov, J. Xia, D.R. Laflen, and C. Grattan, 2000, MASW to investigate anomalous near-surface materials at the Indian Refinery in Lawrenceville, Illinois: Kansas Geological Survey Open-file Report 2000-4.
- Miller, R.D., J. Xia, C.B. Park, and J. Ivanov, 1999, Multichannel analysis of surfaces waves to map bedrock: *Leading Edge*, v. 18, n. 12, p. 1392-1396..
- Mitchell, S.F., 2013, Stratigraphy of the White Limestone of Jamaica: *Bulletin de la Société Géologique de France*, v. 184, p. 111-118.
- Park, C.B., and R.D. Miller, 2005, Seismic Characterization of Wind Turbine Sites in Kansas by the MASW Method: Kansas Geological Survey Open-file Report 2005-23.
- Park, C.B., R.D. Miller, and J. Xia, 1999, Multi-channel analysis of surface waves (MASW): *Geophysics*, v. 64, no. 3, p. 800-808.
- Porter, A.R.D., J.H. Bateson, and N. McFarlane, 1974, Kellits, Geological Sheet 15, 1:50,000 maps with side margin notes: Mines and Geology Division, Jamaica.
- Robinson, E., 1994, Caribbean geology: an introduction, in S.K. Donovan and T.A. Jackson, eds.: University of the West Indies Press, p. 111-127.
- Stokoe II, K.H., S.G. Wright, J.S. Bay, and J.M. Roësset, 1994, Characterization of geotechnical sites by SASW method, in Geophysical characterization of sites, edited by R.D. Woods, Oxford, New Delhi.
- Xia, J., R.D. Miller, and C.B. Park, 1999, Estimation of near-surface shear-wave velocity by inversion of Rayleigh wave: *Geophysics*, v. 64, n. 3, p. 691-700.

APPENDIX A 2-D Vs Profiles

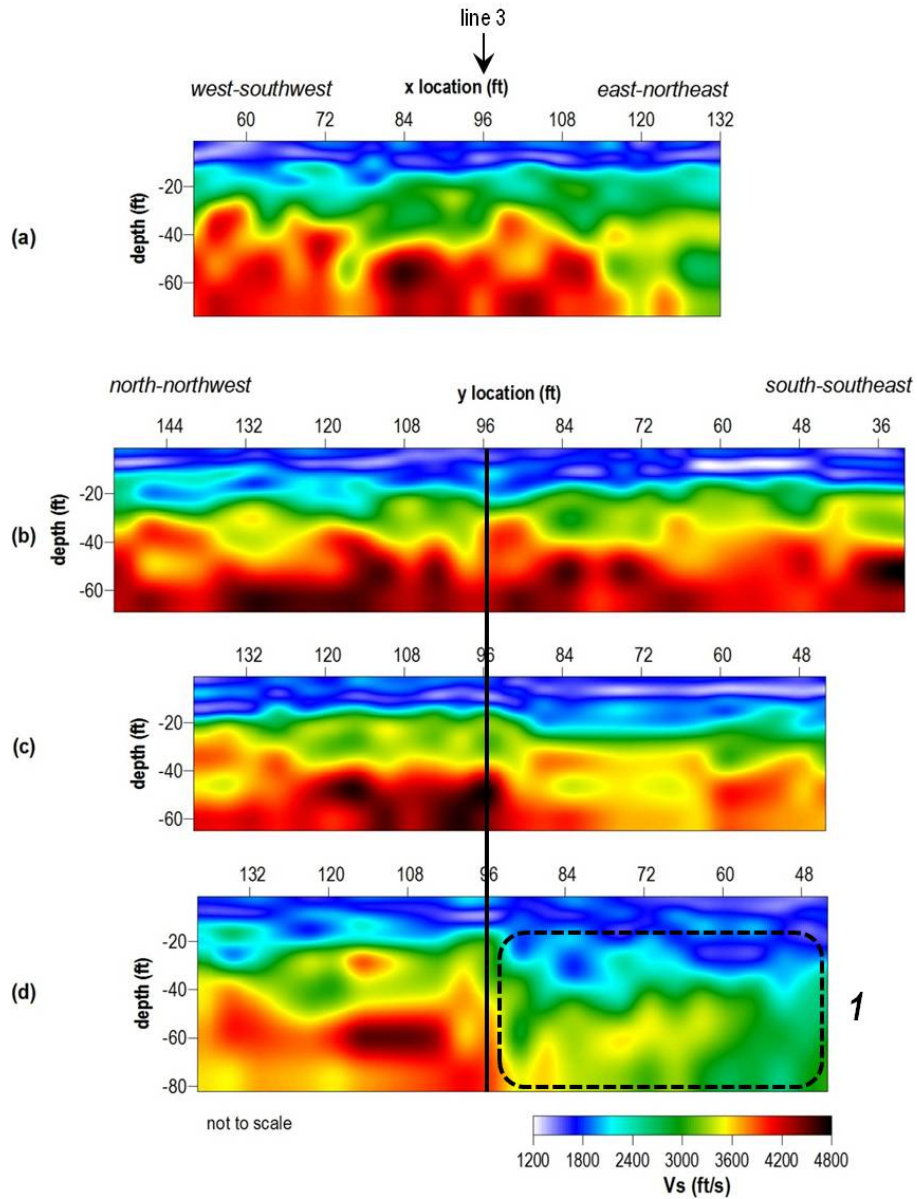


Figure A-1. 2-D Vs profiles obtained using MASW at site T1 for (a) line 1, (b) line 2, (c) line 3, and (d) line 4. The solid black line on lines 2-4 indicates the line 1 intersection. Arrows above line 1 indicated the line 2-4 intersections. Numbered, dashed black boxes indicate potential anomalies.

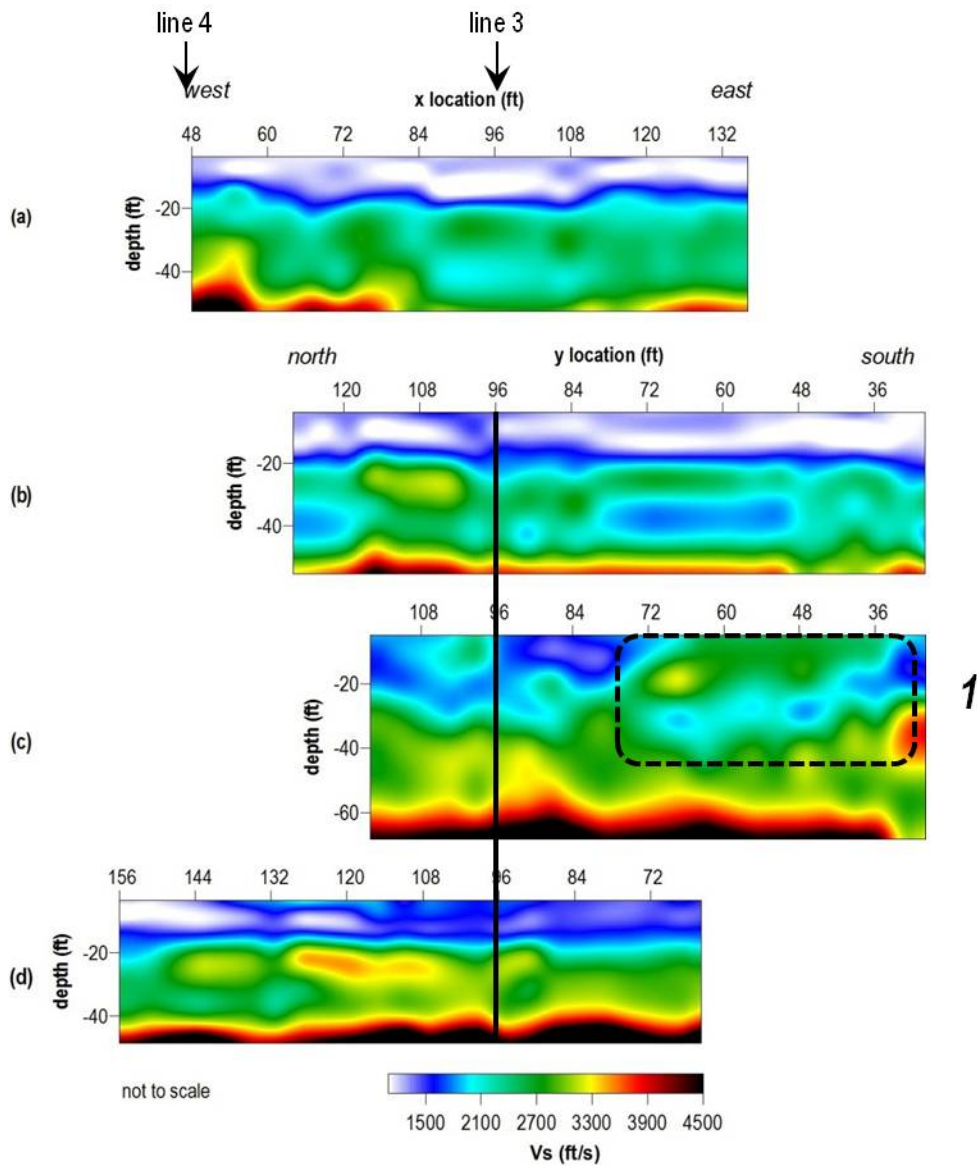


Figure A-2. 2-D V_s profiles obtained using MASW at site T2 for (a) line 1, (b) line 2, (c) line 3, and (d) line 4. The solid black line on lines 2-4 indicates the line 1 intersection. Arrows above line 1 indicated the line 2-4 intersections. Numbered, dashed black boxes indicate potential anomalies.

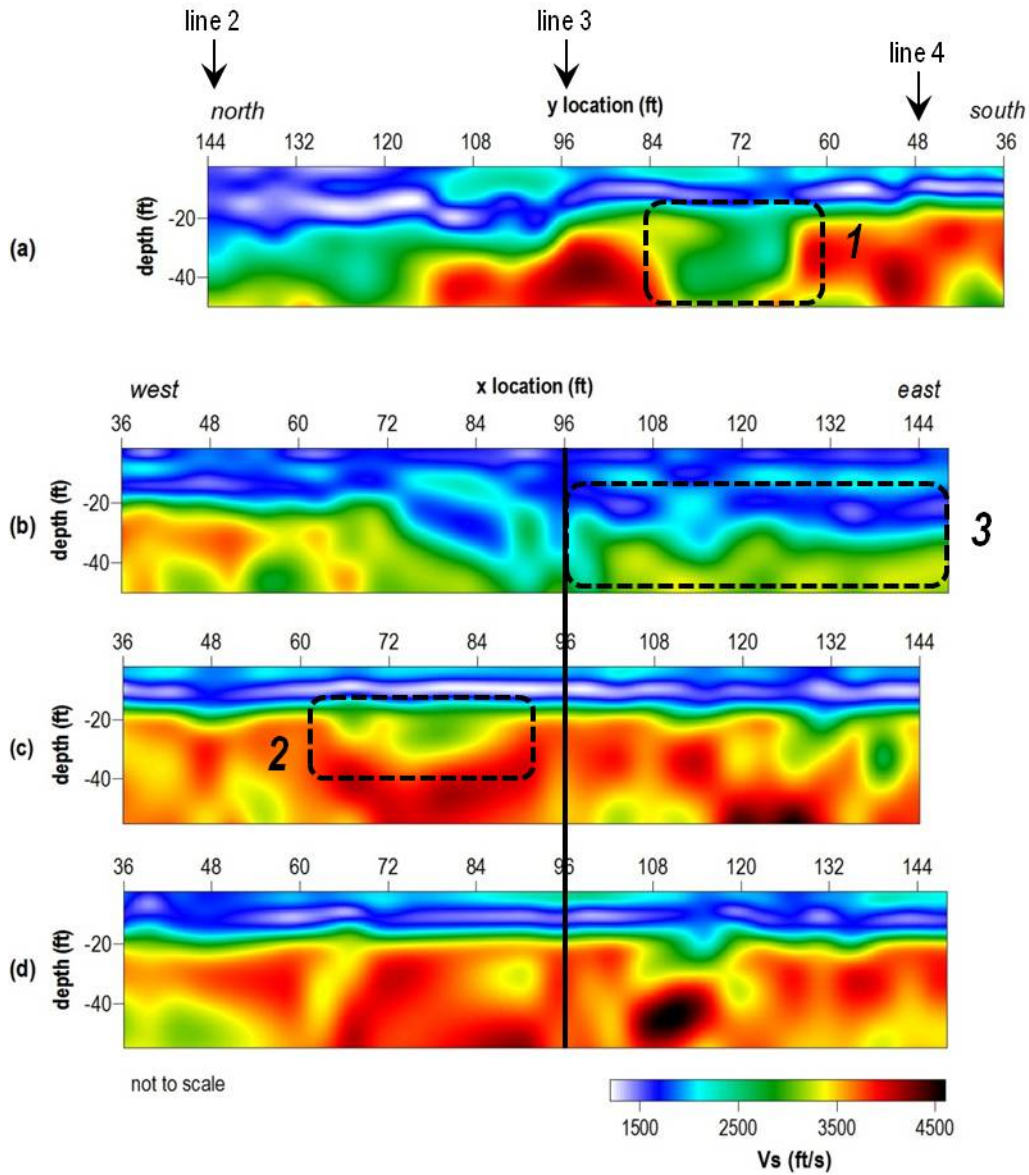


Figure A-3. 2-D Vs profiles obtained using MASW at site T3 for (a) line 1, (b) line 2, (c) line 3, and (d) line 4. The solid black line on lines 2-4 indicates the line 1 intersection. Arrows above line 1 indicated the line 2-4 intersections. Numbered, dashed black boxes indicate potential anomalies.

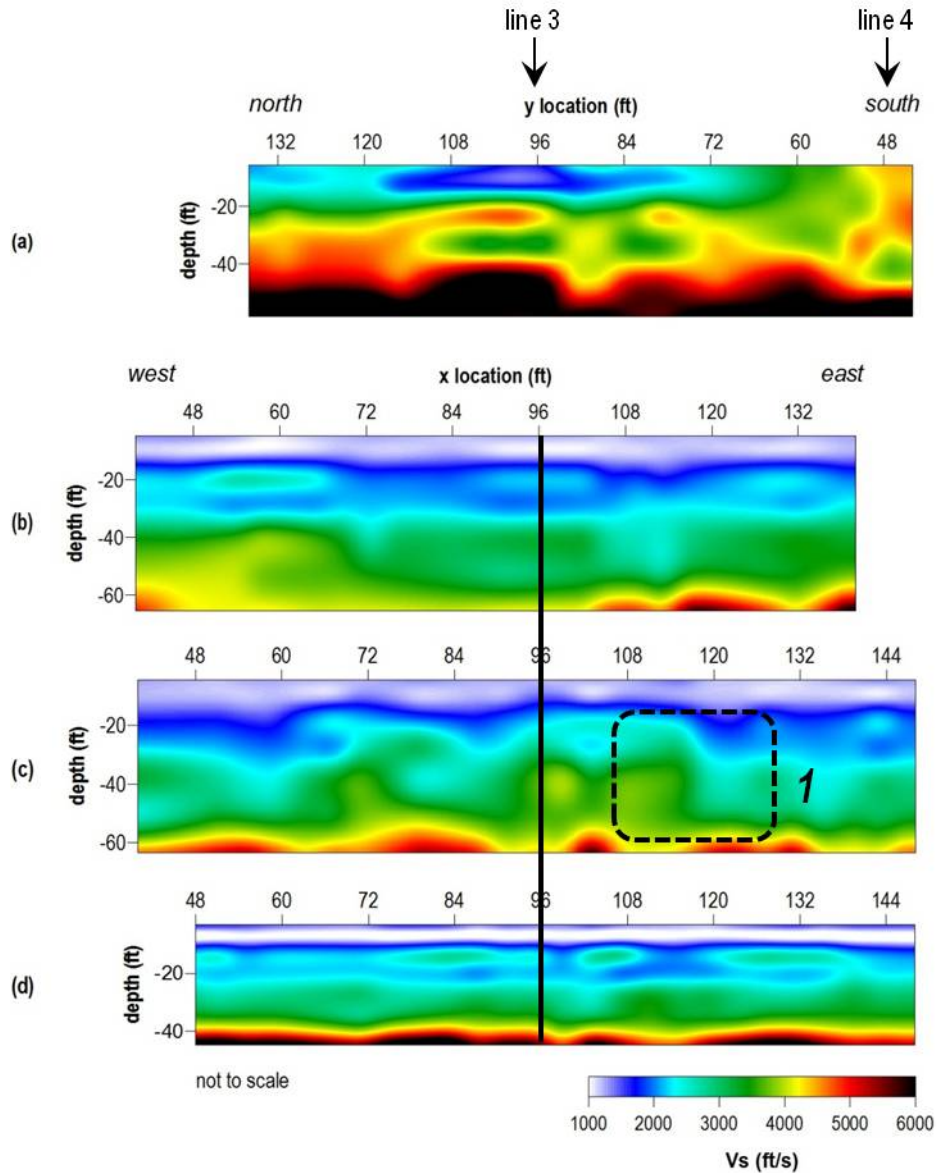


Figure A-4. 2-D Vs profiles obtained using MASW at site T4 for (a) line 1, (b) line 2, (c) line 3, and (d) line 4. The solid black line on lines 2-4 indicates the line 1 intersection. Arrows above line 1 indicated the line 2-4 intersections. Numbered, dashed black boxes indicate potential anomalies.

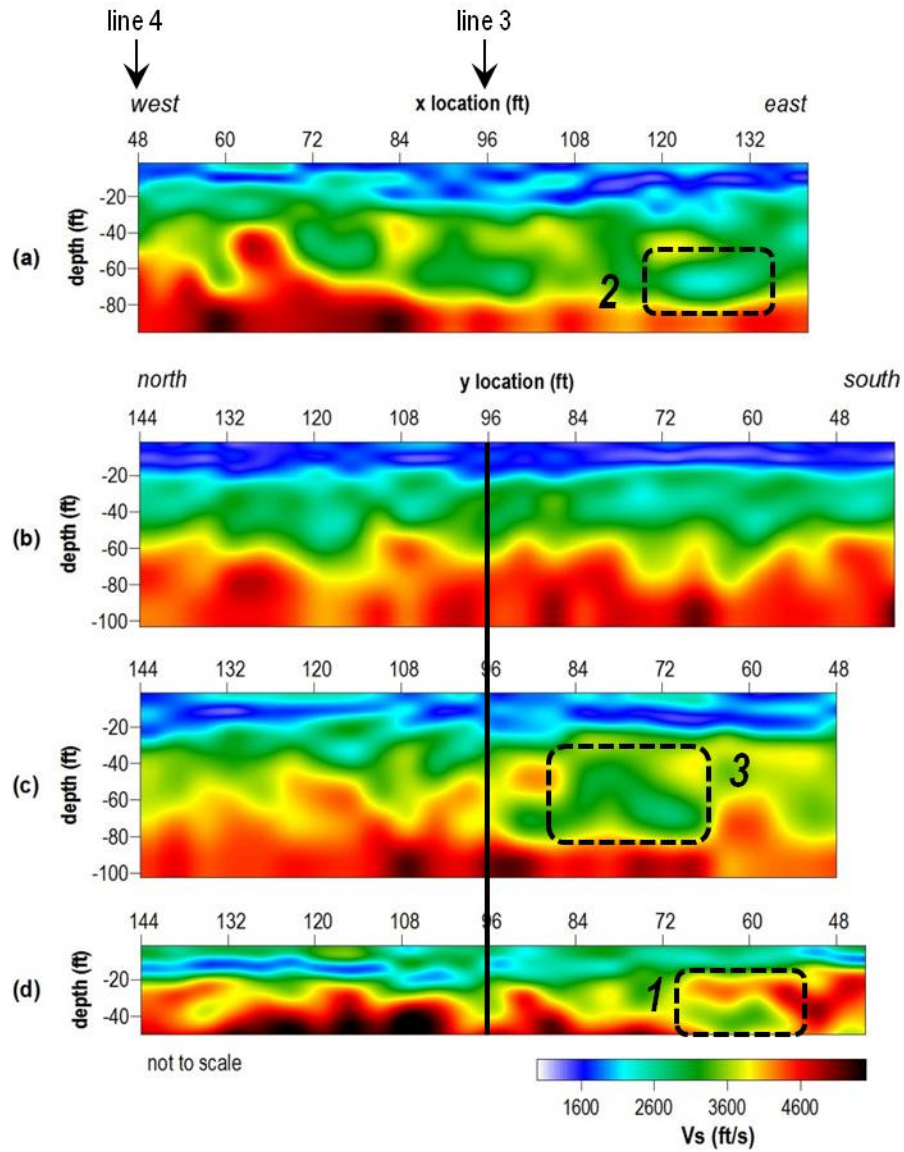


Figure A-5. 2-D Vs profiles obtained using MASW at site T5 for (a) line 1, (b) line 2, (c) line 3, and (d) line 4. The solid black line on lines 2-4 indicates the line 1 intersection. Arrows above line 1 indicated the line 2-4 intersections. Numbered, dashed black boxes indicate potential anomalies.

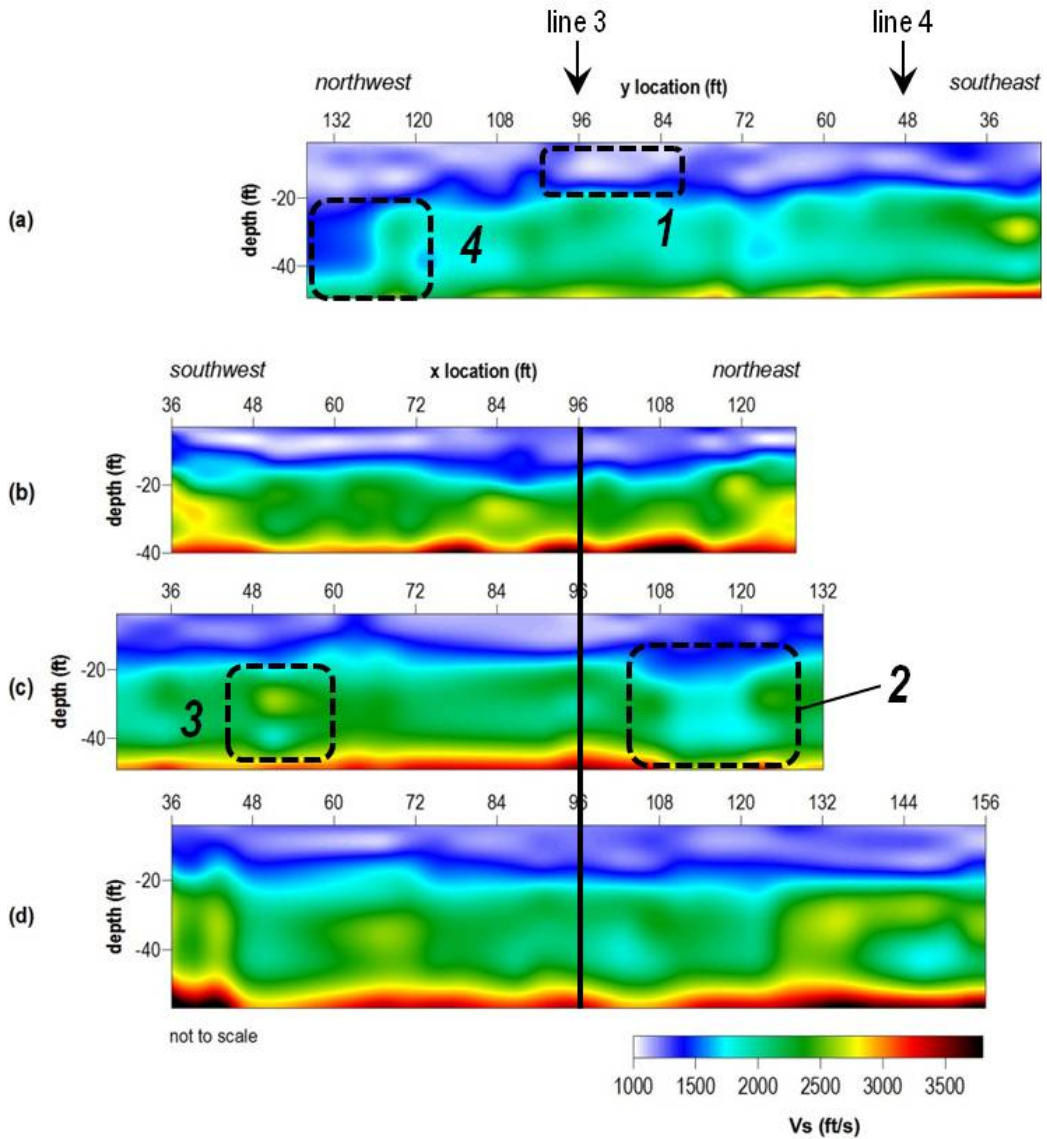


Figure A-6. 2-D Vs profiles obtained using MASW at site T6 for (a) line 1, (b) line 2, (c) line 3, and (d) line 4. The solid black line on lines 2-4 indicates the line 1 intersection. Arrows above line 1 indicated the line 2-4 intersections. Numbered, dashed black boxes indicate potential anomalies.

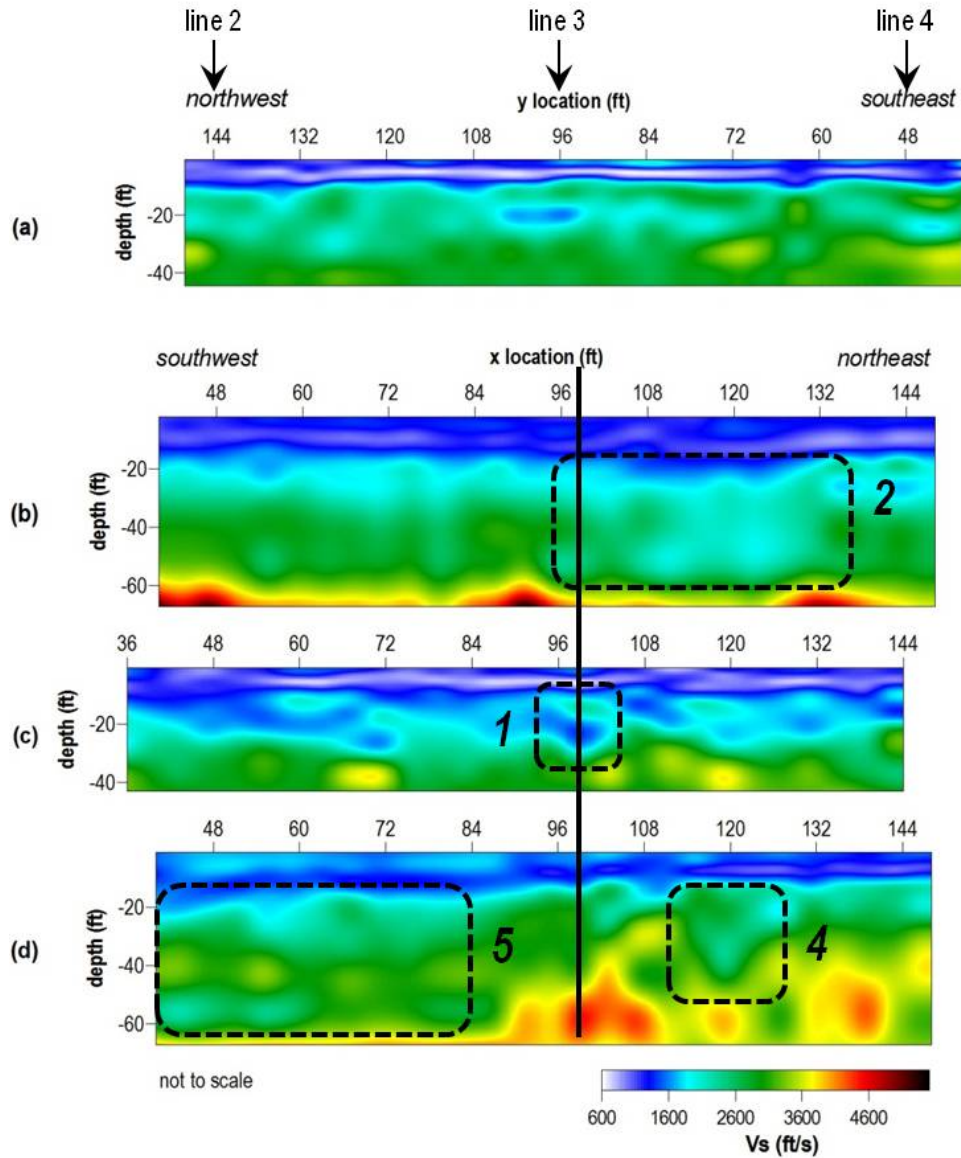


Figure A-7. 2-D Vs profiles obtained using MASW at site T7 for (a) line 1, (b) line 2, (c) line 3, and (d) line 4. The solid black line on lines 2-4 indicates the line 1 intersection. Arrows above line 1 indicated the line 2-4 intersections. Numbered, dashed black boxes indicate potential anomalies.

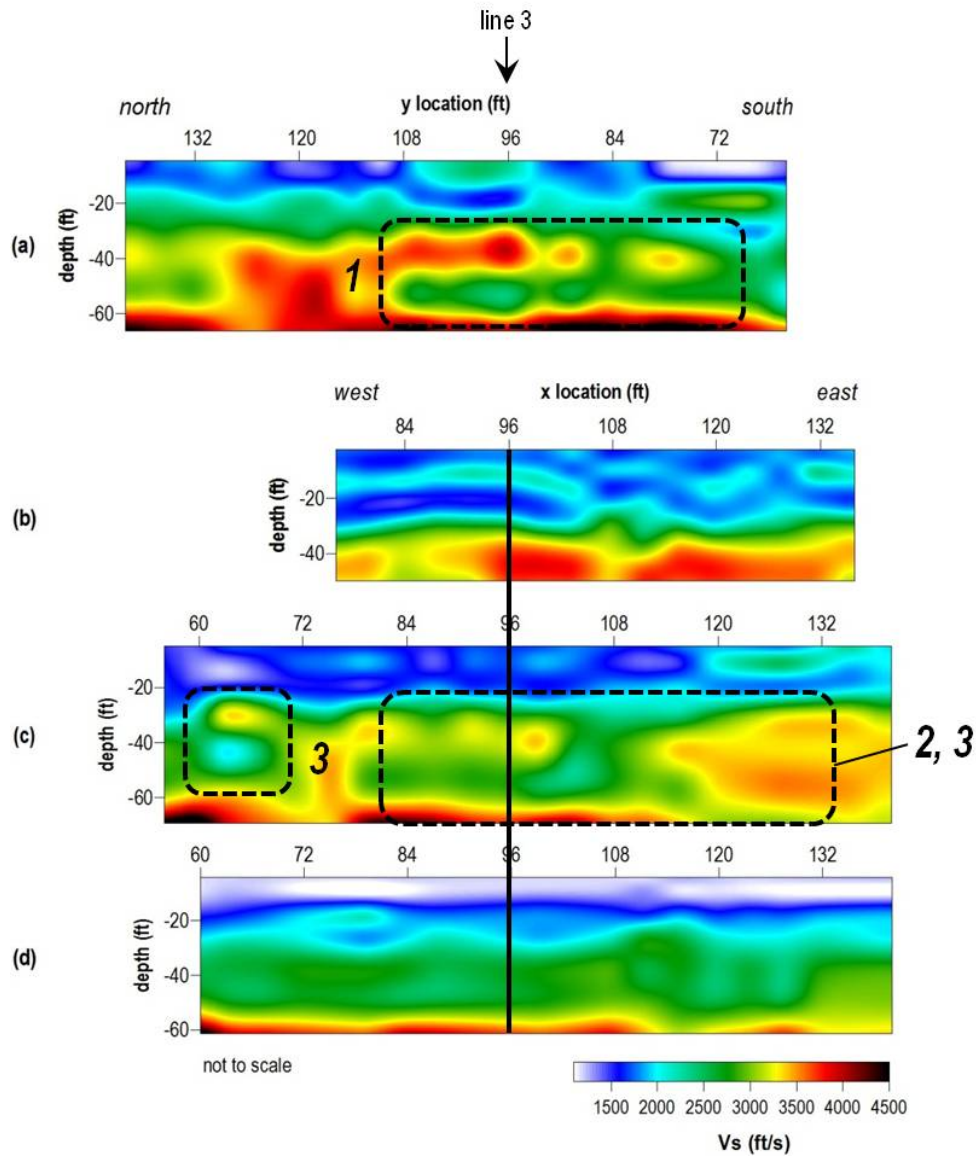


Figure A-8. 2-D V_s profiles obtained using MASW at site T8 for (a) line 1, (b) line 2, (c) line 3, and (d) line 4. The solid black line on lines 2-4 indicates the line 1 intersection. Arrows above line 1 indicated the line 2-4 intersections. Numbered, dashed black boxes indicate potential anomalies. Final processing reveals that anomalies 1, 2, and 3 identified during preliminary analysis may be related to the same structure.

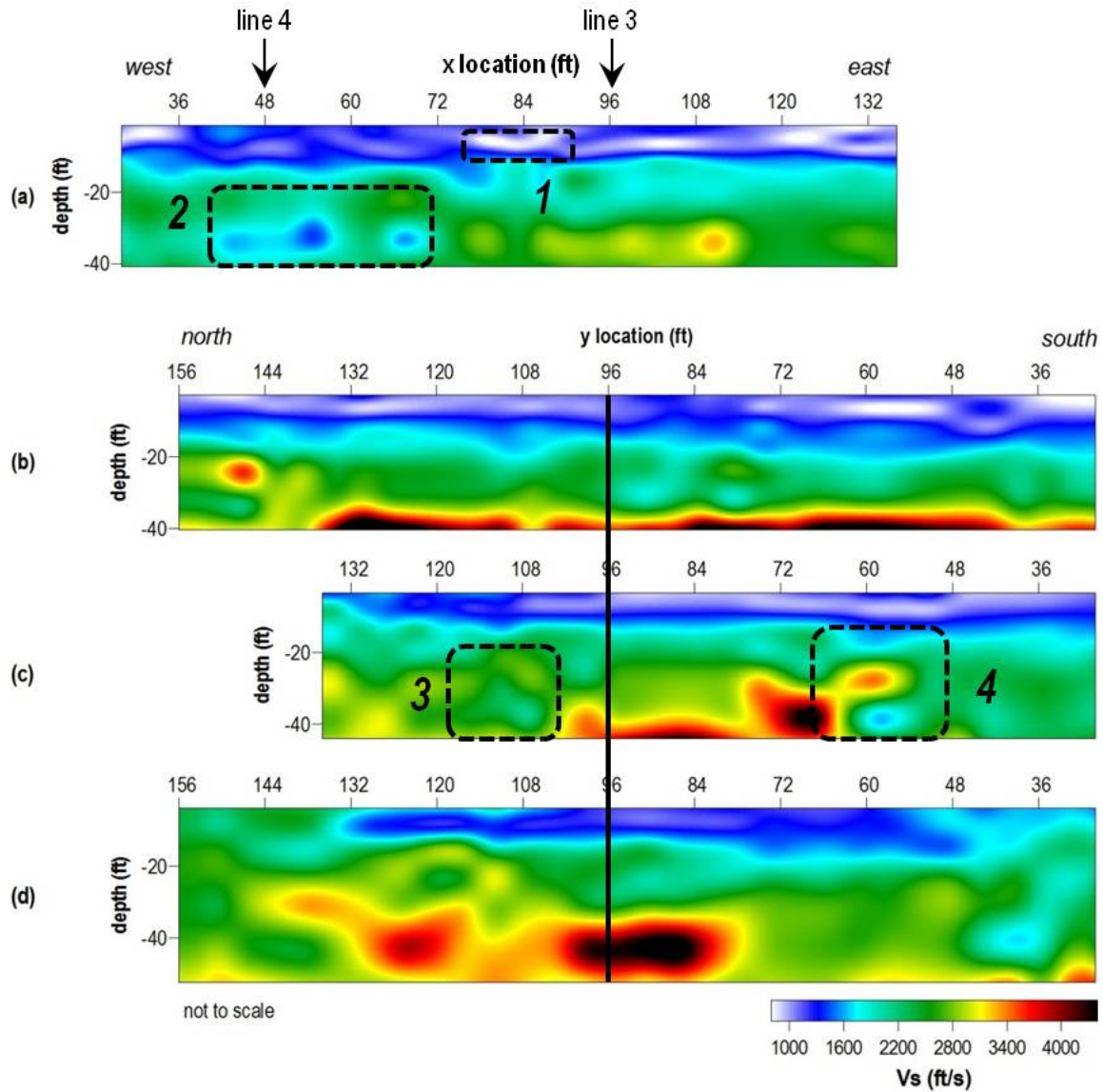


Figure A-9. 2-D Vs profiles obtained using MASW at site T9 for (a) line 1, (b) line 2, (c) line 3, and (d) line 4. The solid black line on lines 2-4 indicates the line 1 intersection. Arrows above line 1 indicated the line 2-4 intersections. Numbered, dashed black boxes indicate potential anomalies.

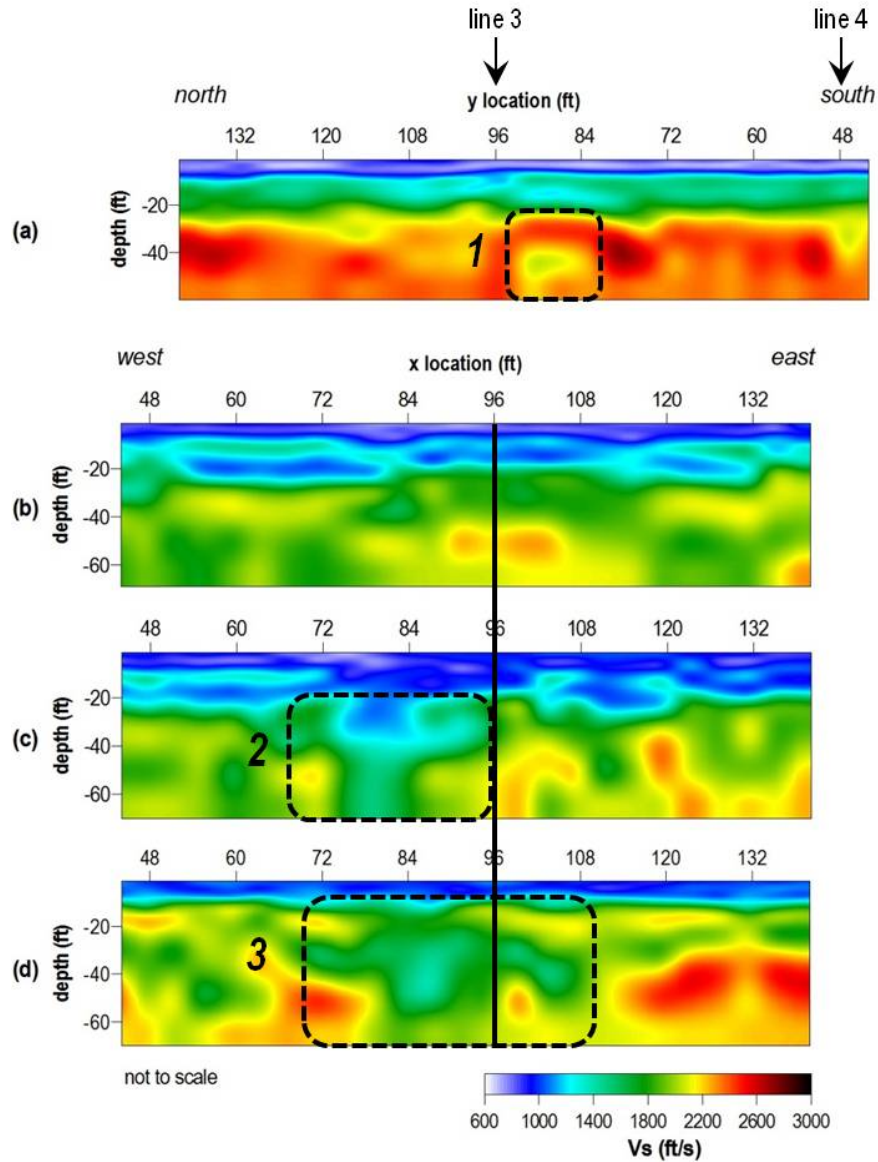


Figure A-10. 2-D Vs profiles obtained using MASW at site T10 for (a) line 1, (b) line 2, (c) line 3, and (d) line 4. The solid black line on lines 2-4 indicates the line 1 intersection. Arrows above line 1 indicated the line 2-4 intersections. Numbered, dashed black boxes indicate potential anomalies.

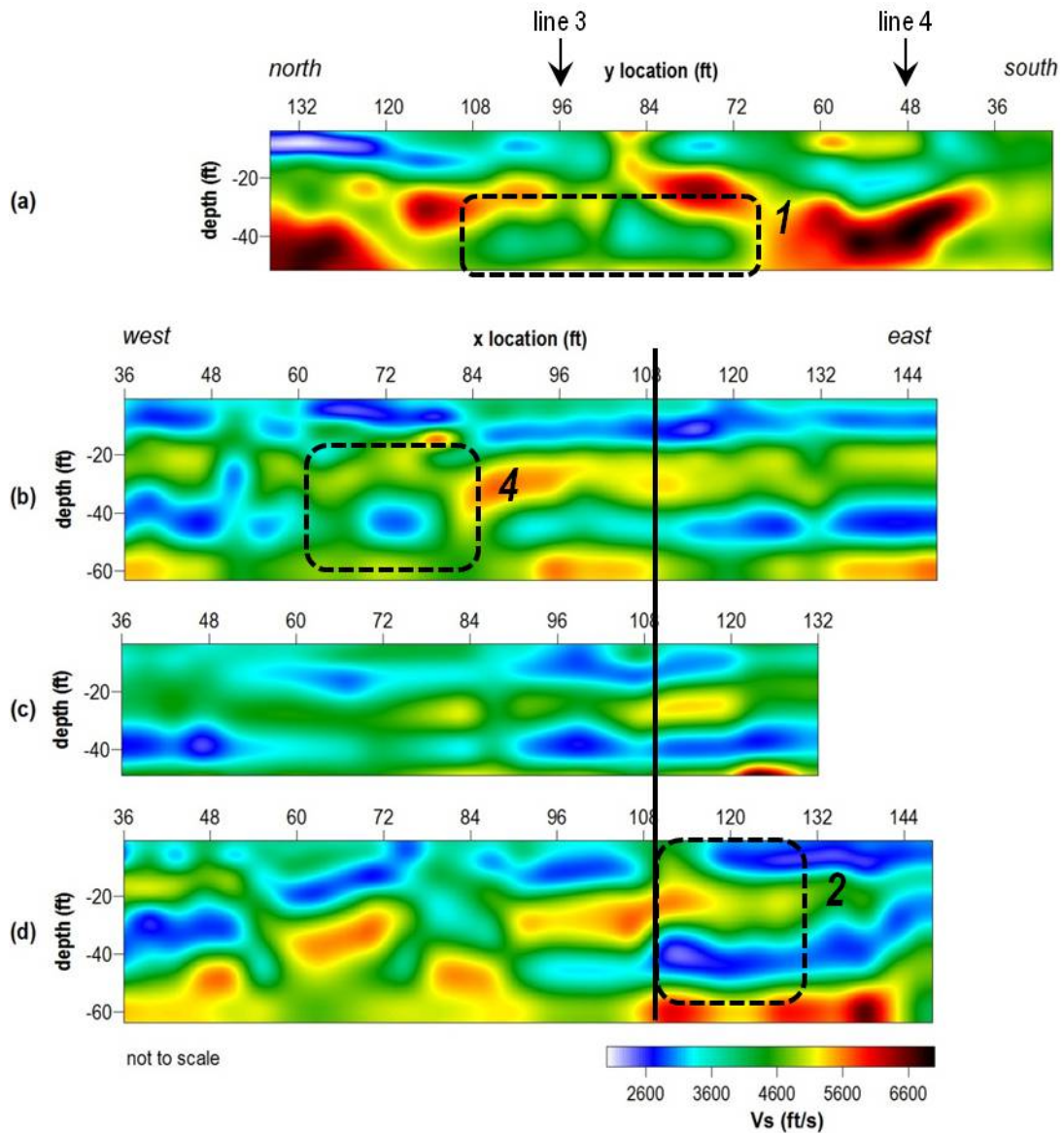


Figure A-11. 2-D Vs profiles obtained using MASW at site T11 for (a) line 1, (b) line 2, (c) line 3, and (d) line 4. The solid black line on lines 2-4 indicates the line 1 intersection. Arrows above line 1 indicated the line 2-4 intersections. Numbered, dashed black boxes indicate potential anomalies.

APPENDIX B
Probability Density Maps

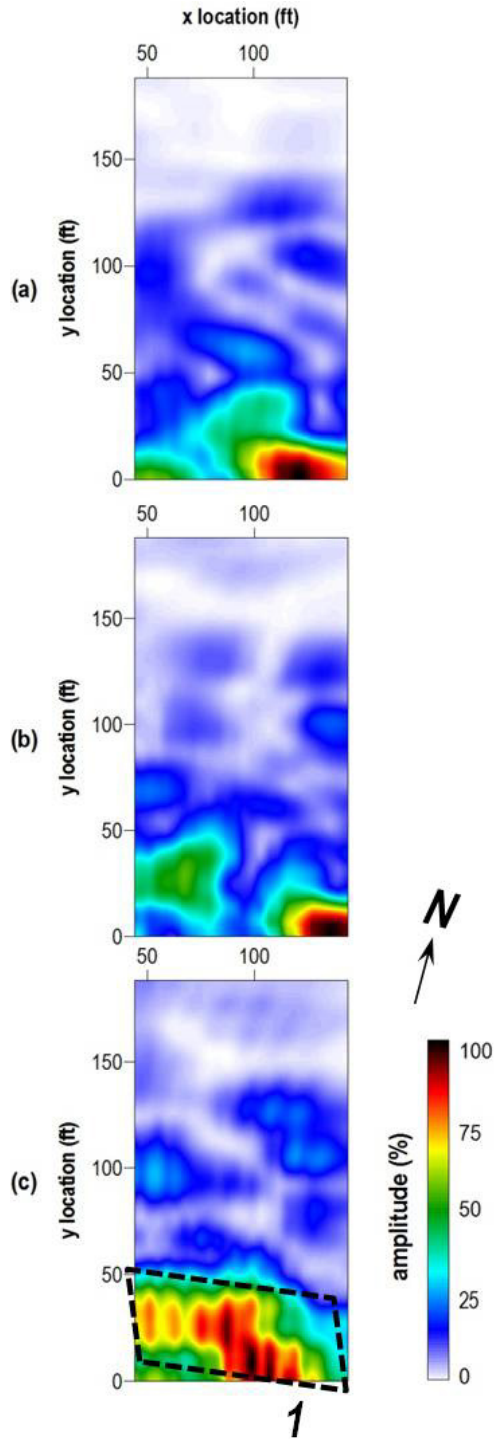


Figure B-1. Probability density maps for site T1 at depths of (a) 10-20 ft, (b) 20-30 ft, and (c) 30-50 ft. Numbered, dashed black boxes indicate potential anomalies.

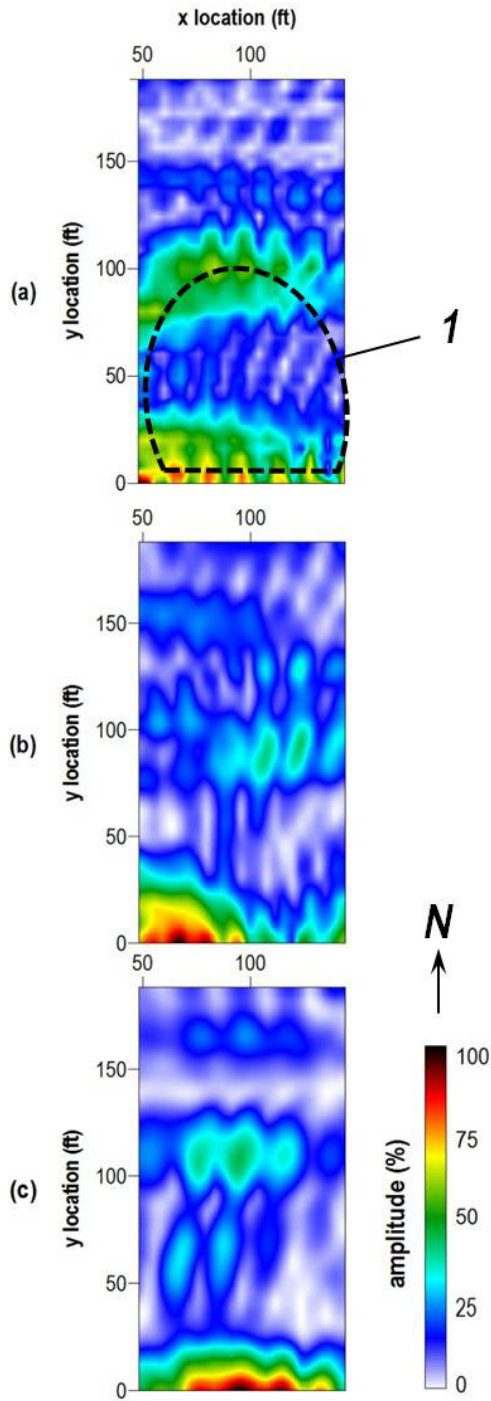


Figure B-2. Probability density maps for site T2 at depths of (a) 10-20 ft, (b) 20-30 ft, and (c) 30-50 ft. Numbered, dashed black boxes indicate potential anomalies.

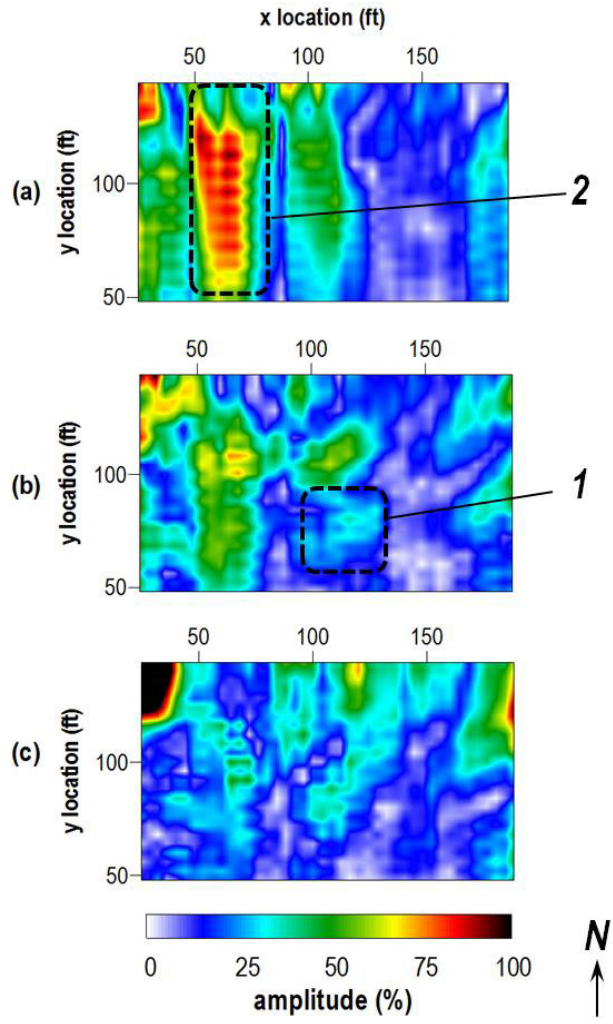


Figure B-3. Probability density maps for site T3 at depths of (a) 10-20 ft, (b) 20-30 ft, and (c) 30-50 ft. Numbered, dashed black boxes indicate potential anomalies.

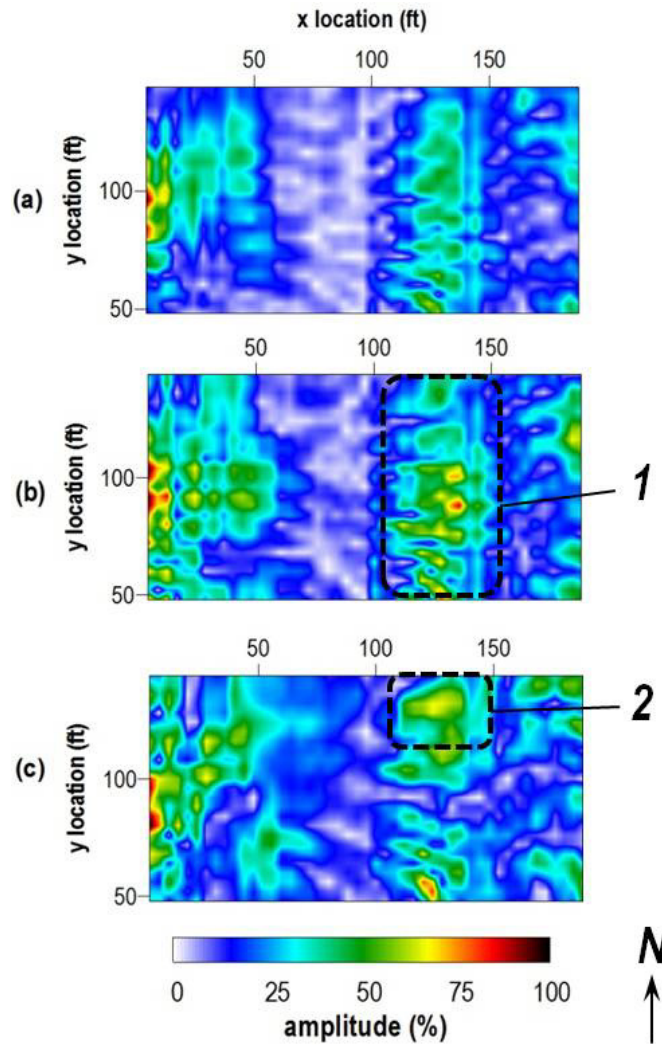


Figure B-4. Probability density maps for site T4 at depths of (a) 10-20 ft, (b) 20-30 ft, and (c) 30-50 ft. Numbered, dashed black boxes indicate potential anomalies.

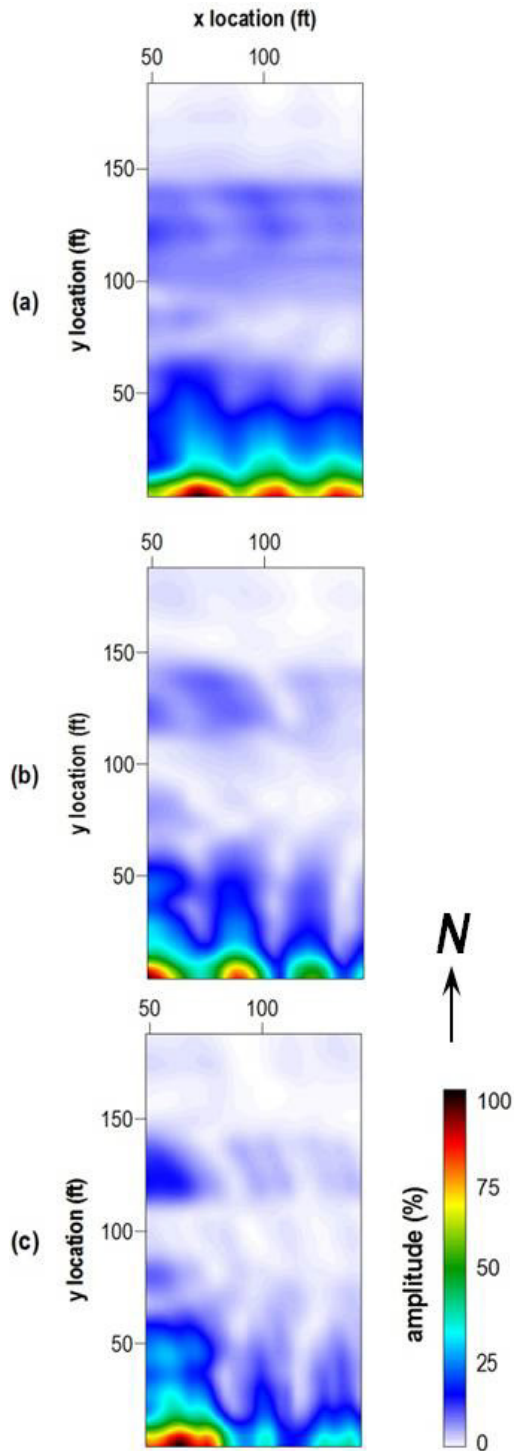


Figure B-5. Probability density maps for site T5 at depths of (a) 10-20 ft, (b) 20-30 ft, and (c) 30-50 ft. Numbered, dashed black boxes indicate potential anomalies.

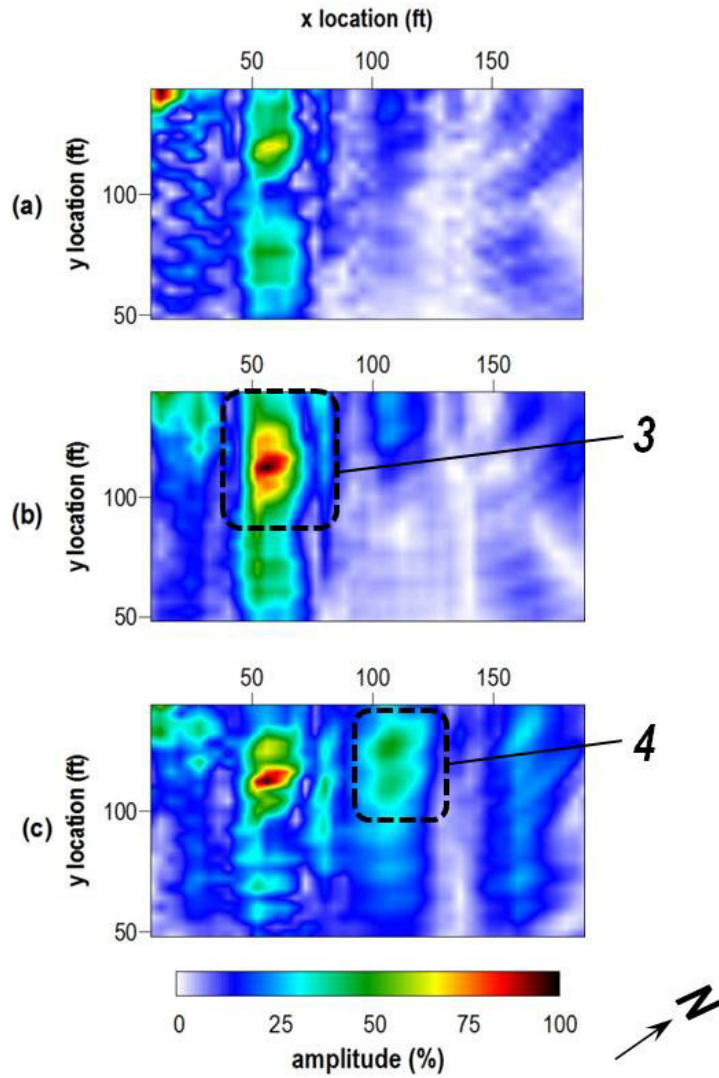


Figure B-6. Probability density maps for site T6 at depths of (a) 10-20 ft, (b) 20-30 ft, and (c) 30-50 ft. Numbered, dashed black boxes indicate potential anomalies.

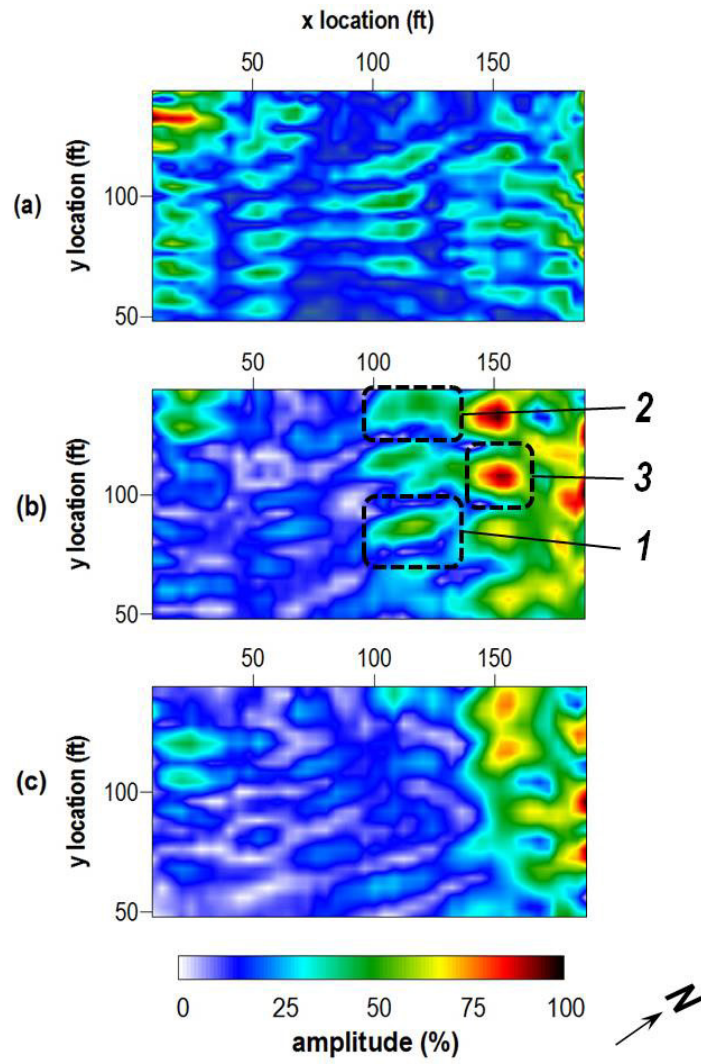


Figure B-7. Probability density maps for site T7 at depths of (a) 10-20 ft, (b) 20-30 ft, and (c) 30-50 ft. Numbered, dashed black boxes indicate potential anomalies.

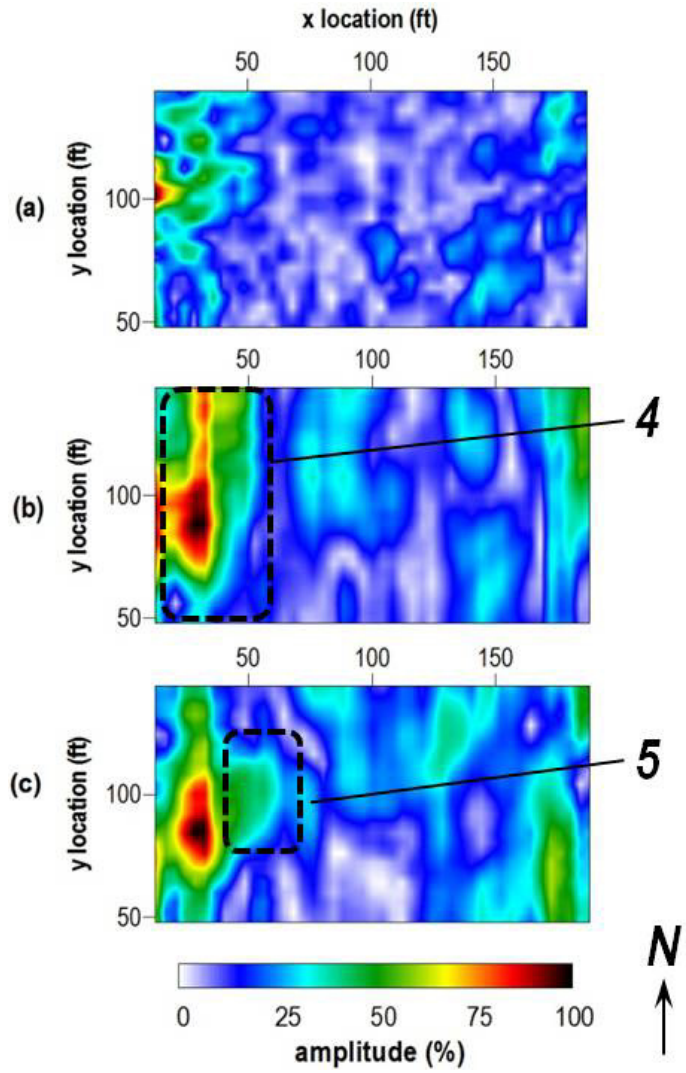


Figure B-8. Probability density maps for site T8 at depths of (a) 10-20 ft, (b) 20-30 ft, and (c) 30-50 ft. Numbered, dashed black boxes indicate potential anomalies.

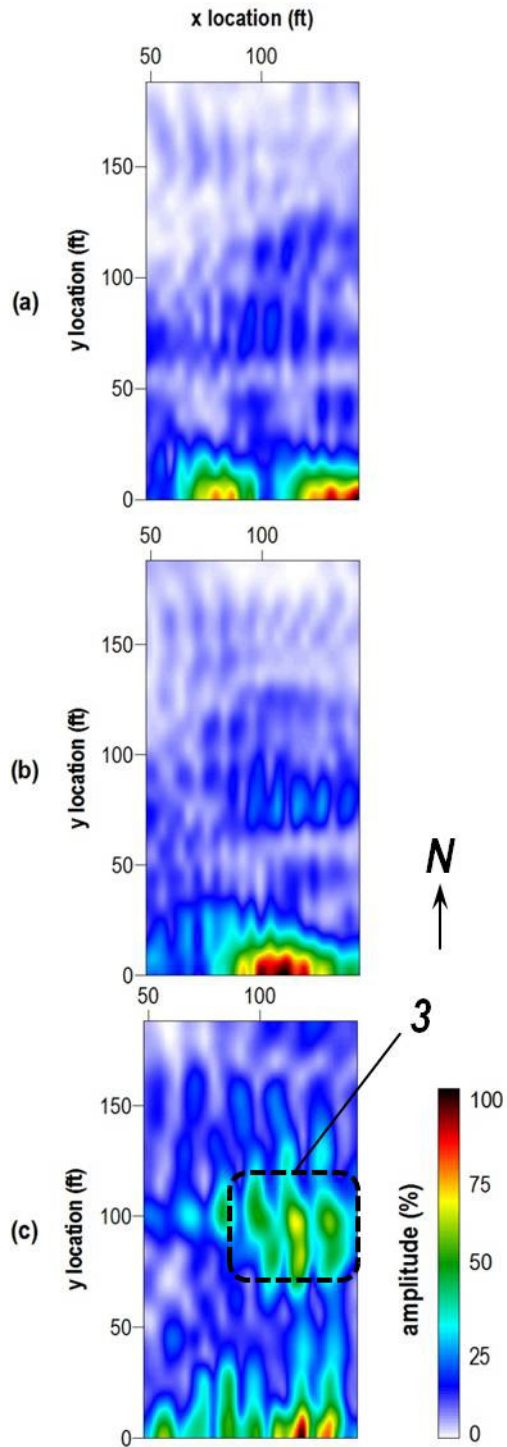


Figure B-9. Probability density maps for site T9 at depths of (a) 10-20 ft, (b) 20-30 ft, and (c) 30-50 ft. Numbered, dashed black boxes indicate potential anomalies.

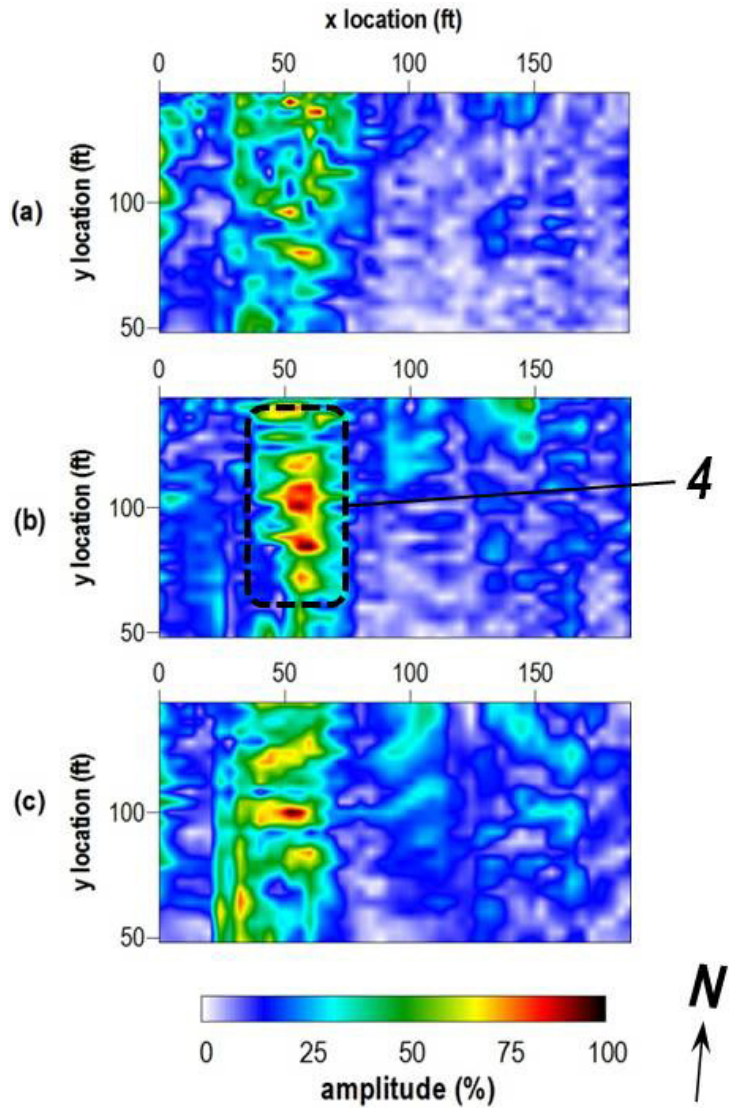


Figure B-10. Probability density maps for site T10 at depths of (a) 10-20 ft, (b) 20-30 ft, and (c) 30-50 ft. Numbered, dashed black boxes indicate potential anomalies.

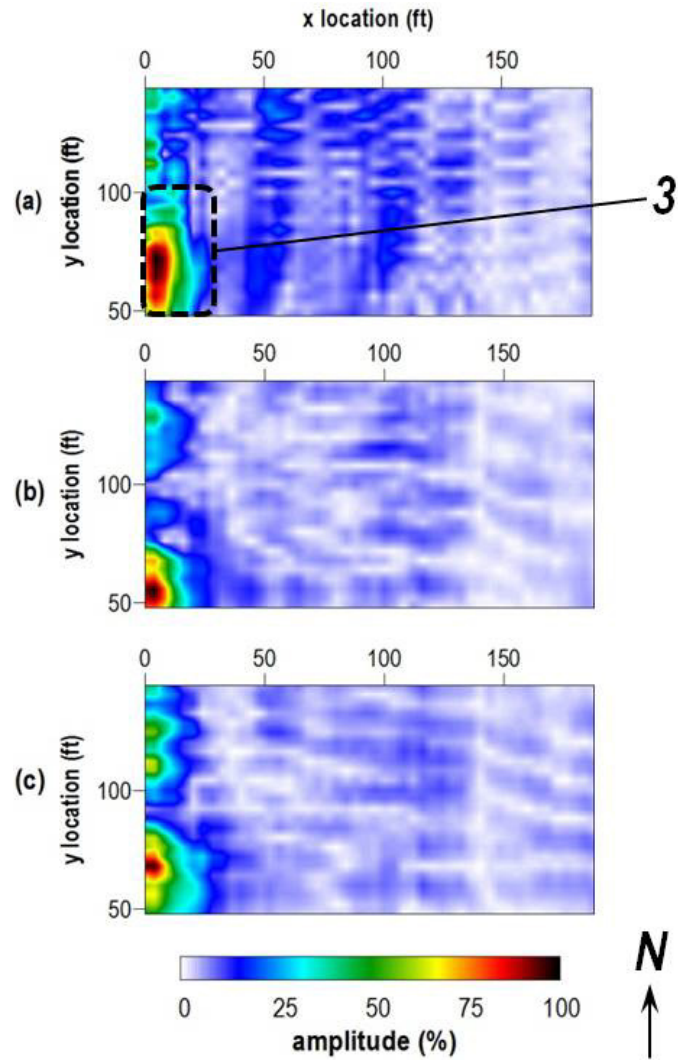


Figure B-11. Probability density maps, generated with a dispersion curve representative of the western portion of site T11, at depths of (a) 10-20 ft, (b) 20-30 ft, and (c) 30-50 ft. Numbered, dashed black boxes indicate potential anomalies.

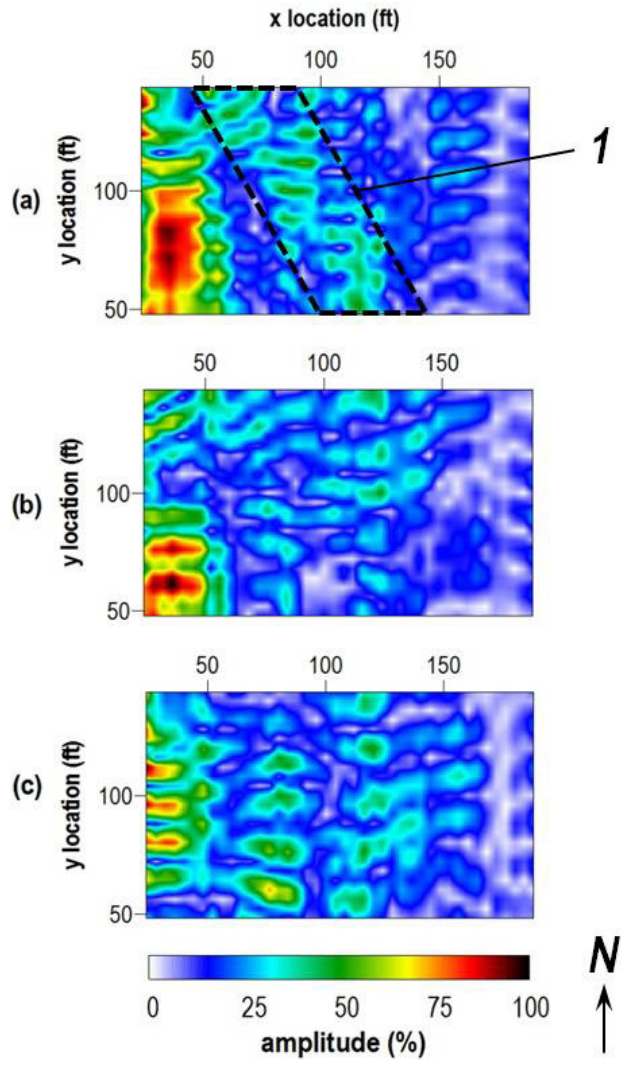


Figure B-12. Probability density maps, generated with a dispersion curve representative of the eastern and central portions of site T11, at depths of (a) 10-20 ft, (b) 20-30 ft, and (c) 30-50 ft. Numbered, dashed black boxes indicate potential anomalies.

APPENDIX C
Average 1-D Vs Profiles

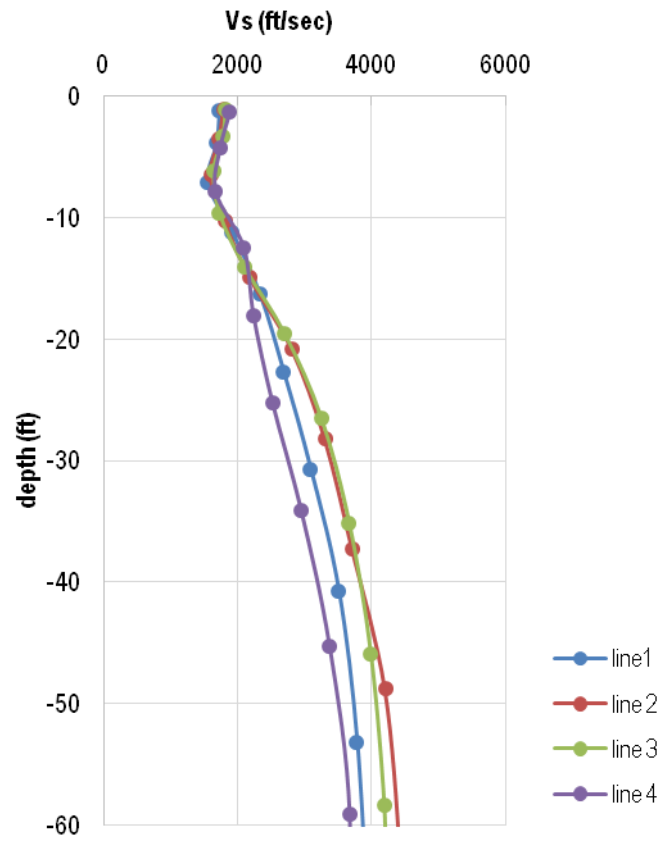


Figure C-1. Average 1-D Vs of the upper 60 ft for each line acquired at site T1.

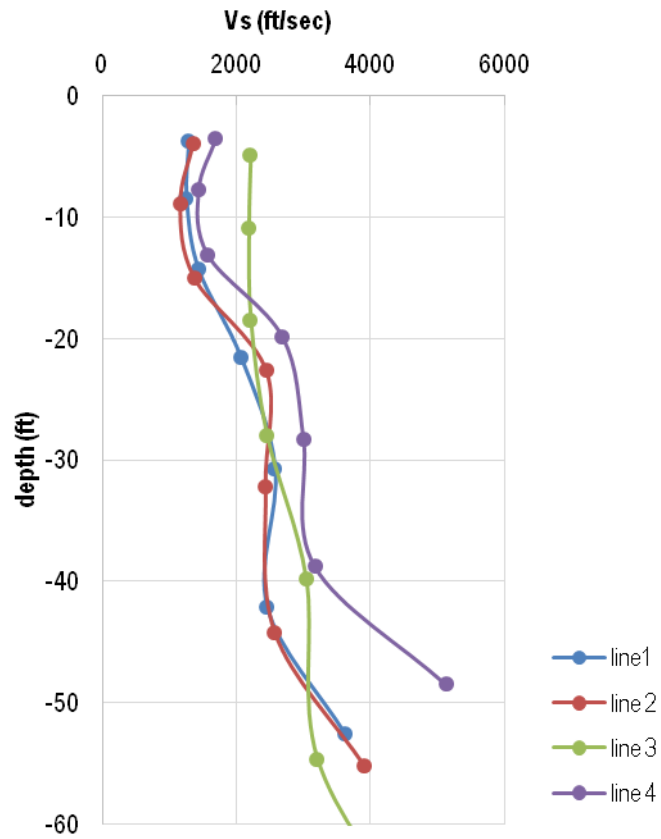


Figure C-2. Average 1-D Vs of the upper 60 ft for each line acquired at site T2.

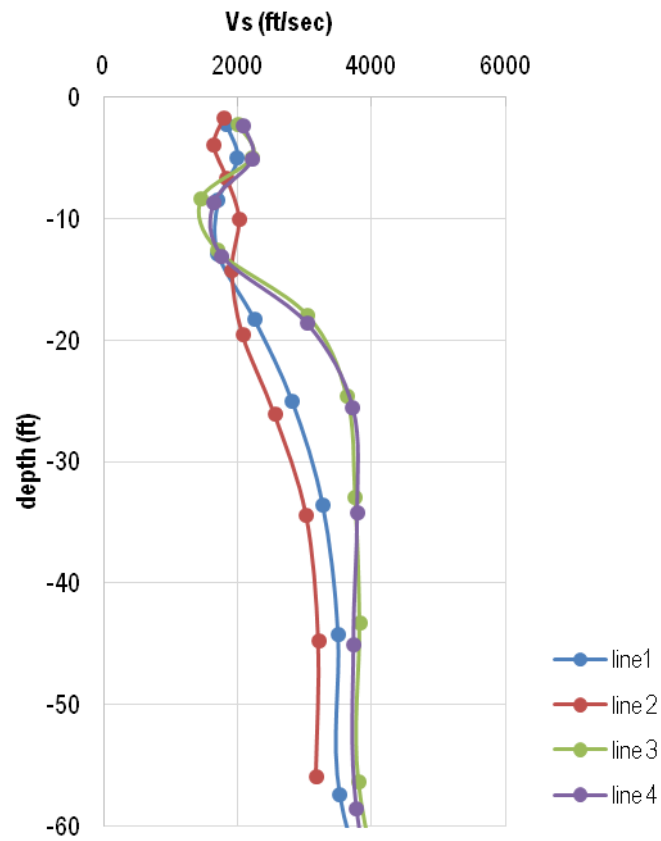


Figure C-3. Average 1-D Vs of the upper 60 ft for each line acquired at site T3.

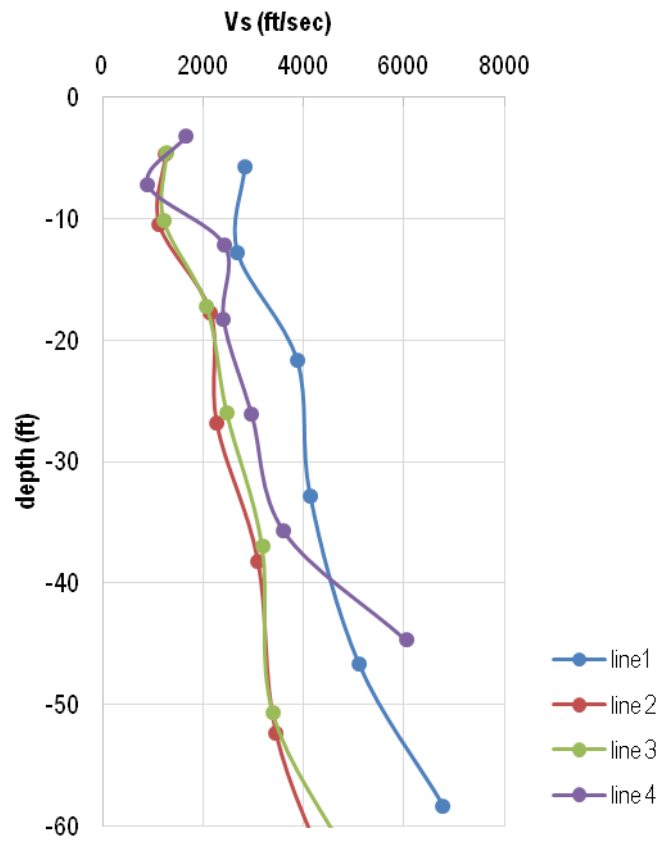


Figure C-4. Average 1-D Vs of the upper 60 ft for each line acquired at site T4.

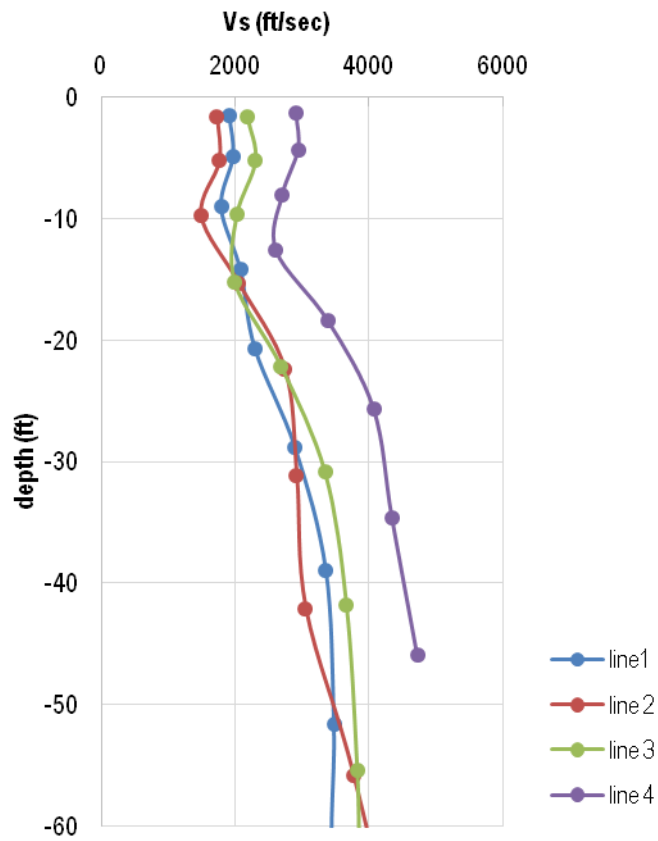


Figure C-5. Average 1-D Vs of the upper 60 ft for each line acquired at site T5.

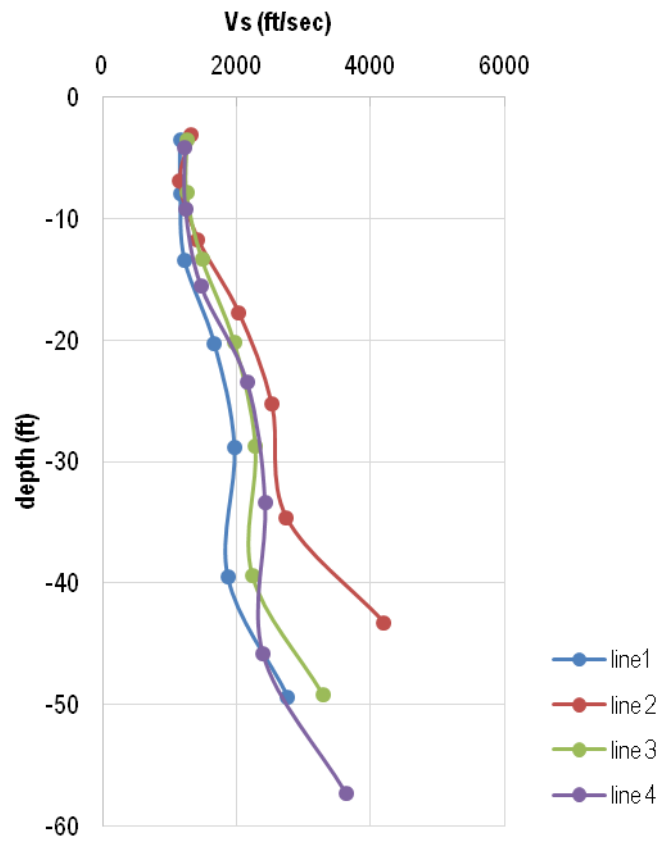


Figure C-6. Average 1-D Vs of the upper 60 ft for each line acquired at site T6.

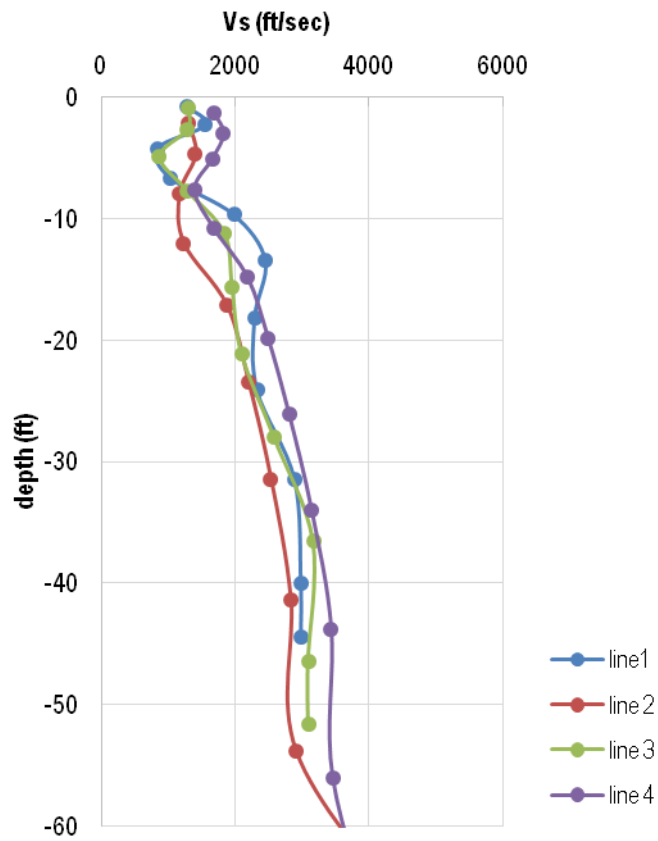


Figure C-7. Average 1-D Vs of the upper 60 ft for each line acquired at site T7.

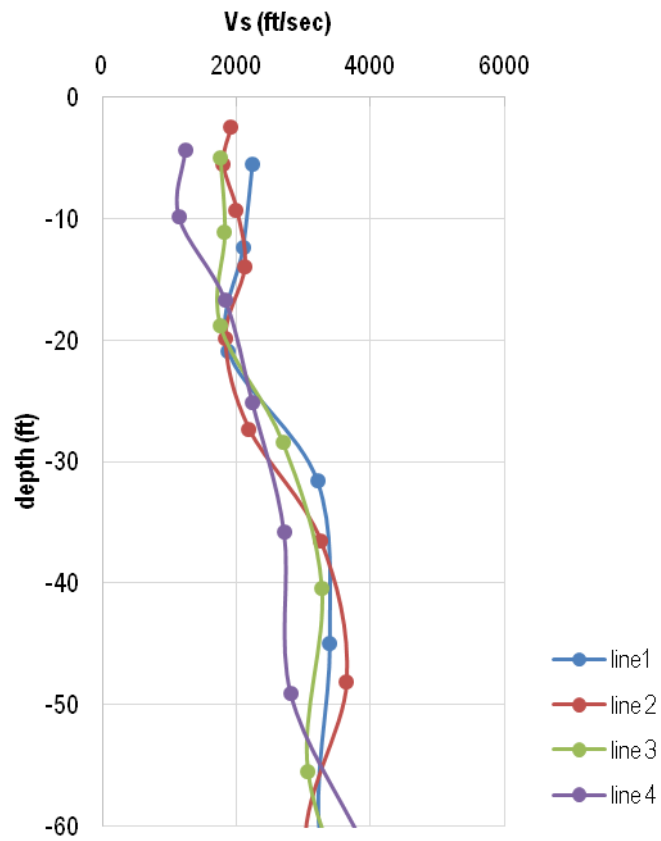


Figure C-8. Average 1-D Vs of the upper 60 ft for each line acquired at site T8.

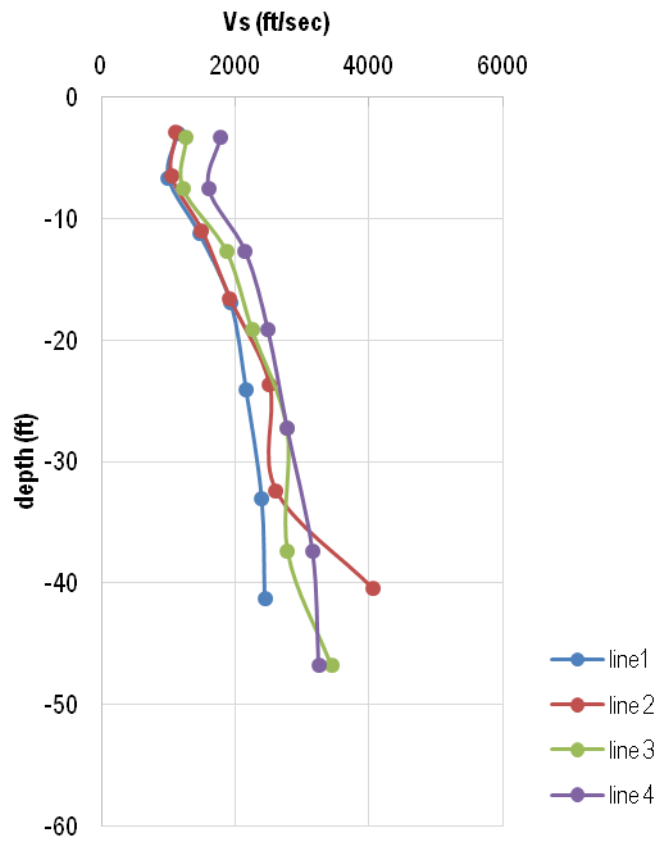


Figure C-9. Average 1-D Vs of the upper 60 ft for each line acquired at site T9.

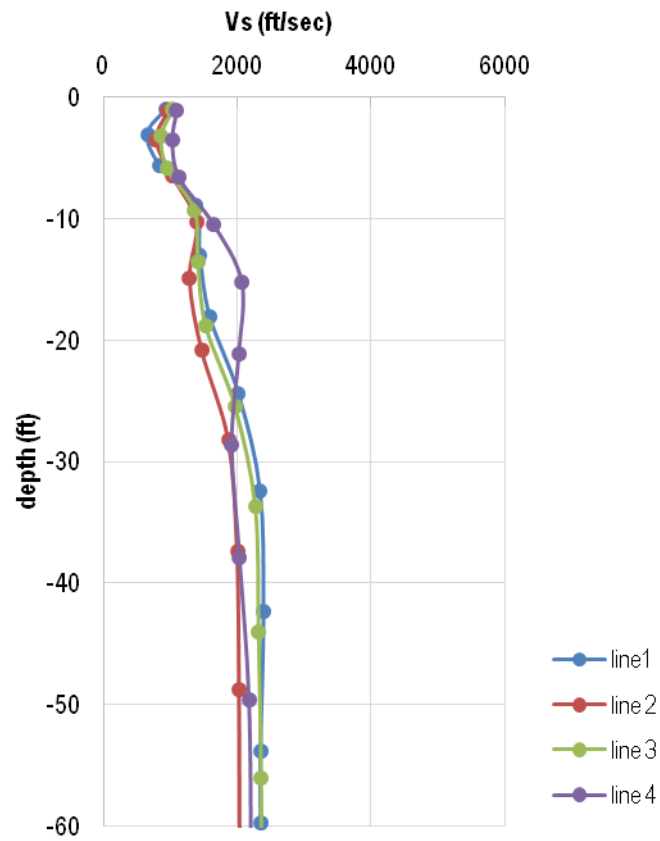


Figure C-10. Average 1-D Vs of the upper 60 ft for each line acquired at site T10.

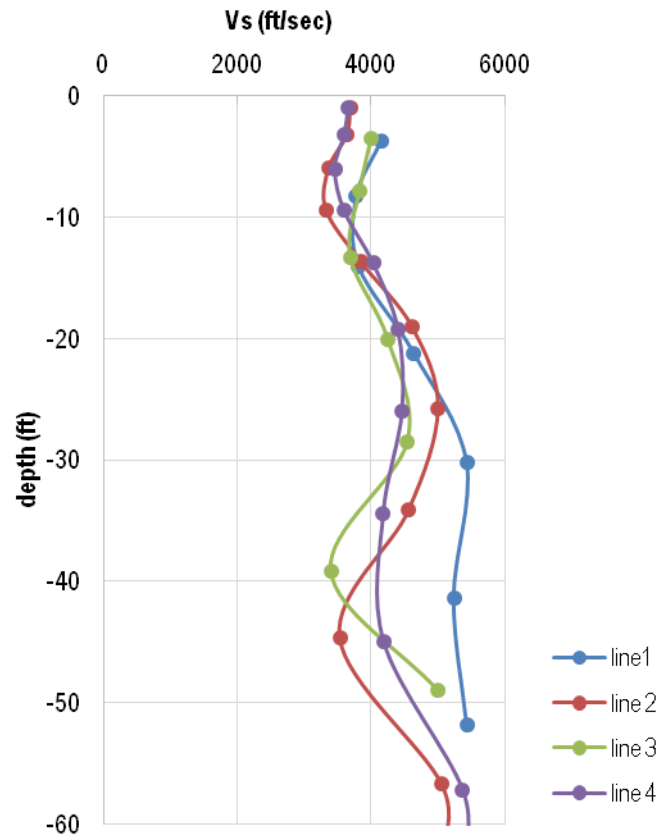


Figure C-11. Average 1-D Vs of the upper 60 ft for each line acquired at site T11.

APPENDIX D
Vs Fence Diagrams

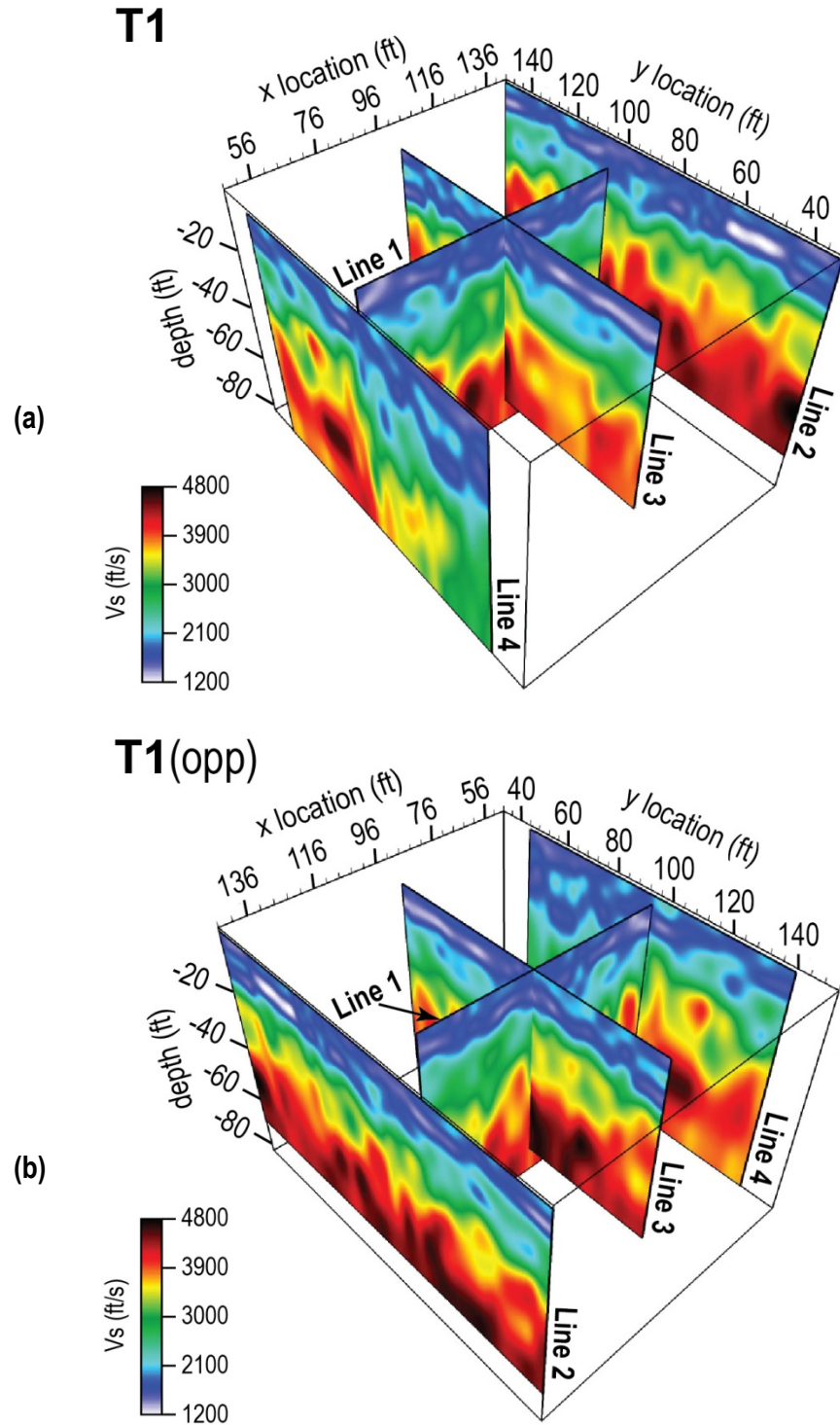


Figure D-1. Fence diagrams of 2-D Vs profiles at site T1 as viewed from (a) the perspective illustrated in Figure 8a, and (b) from the opposite (opp) corner of the site perimeter (Figure 8b).

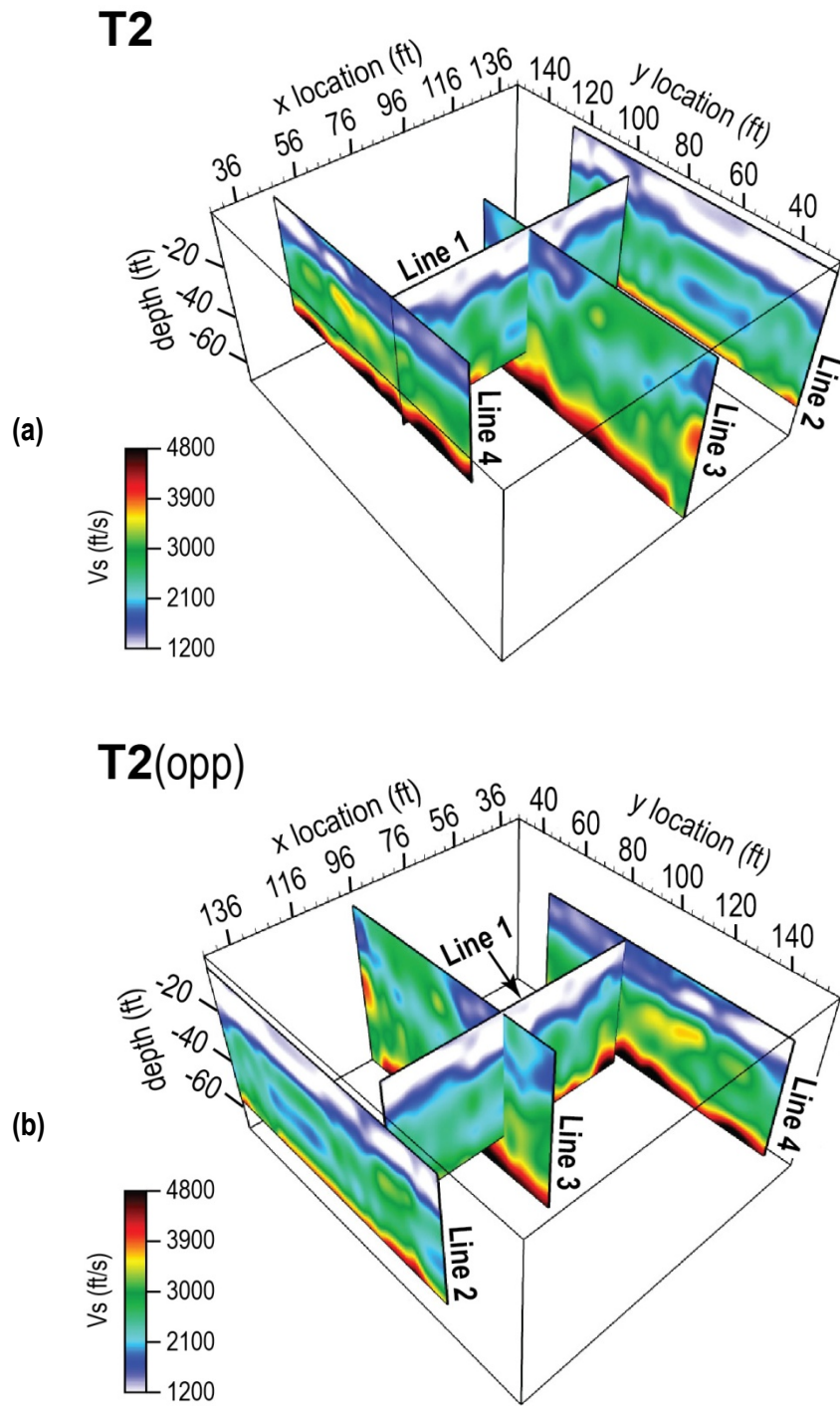


Figure D-2. Fence diagrams of 2-D Vs profiles at site T2 as viewed from (a) the perspective illustrated in Figure 8a, and (b) from the opposite (opp) corner of the site perimeter (Figure 8b).

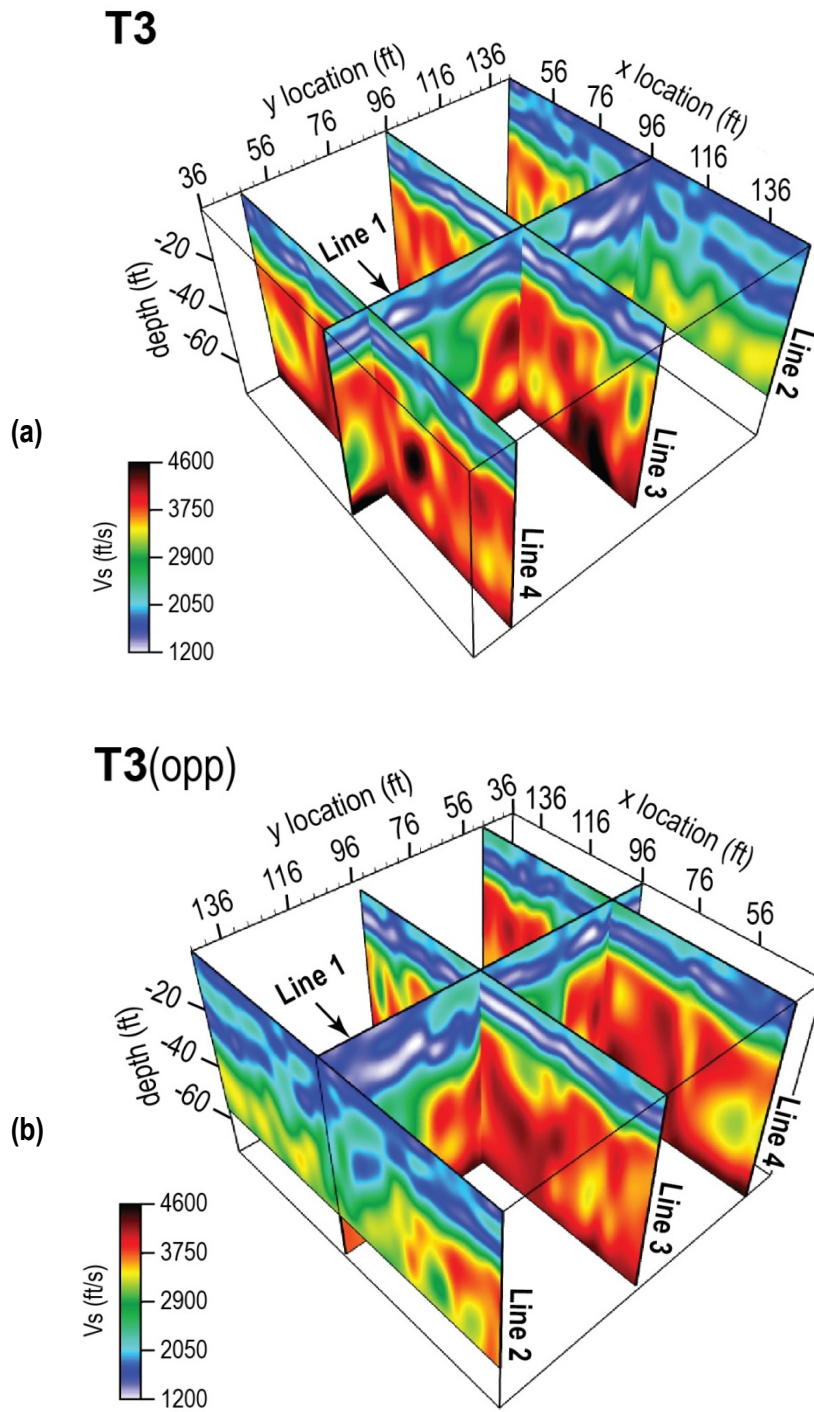
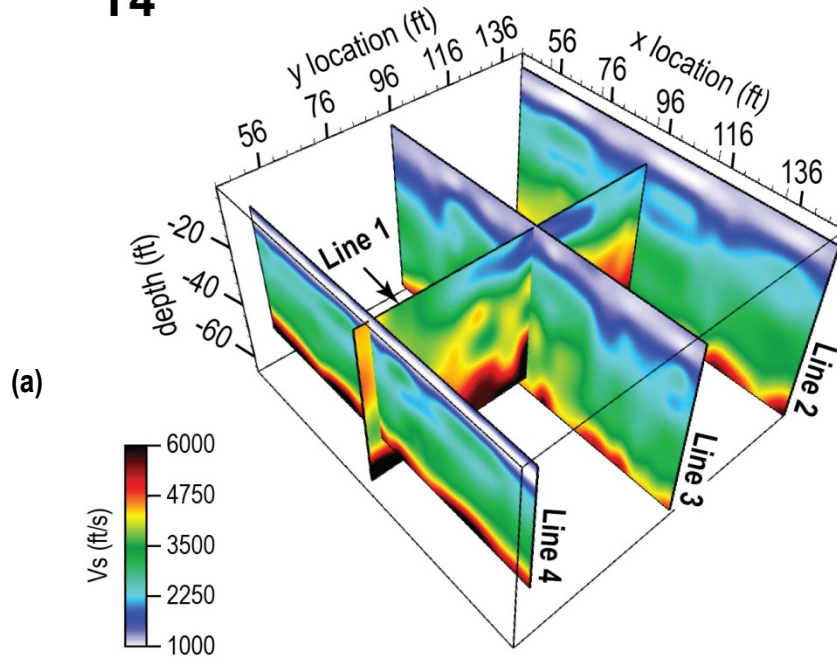


Figure D-3. Fence diagrams of 2-D V_s profiles at site T3 as viewed from (a) the perspective illustrated in Figure 8a, and (b) from the opposite (opp) corner of the site perimeter (Figure 8b).

T4



T4(opp)

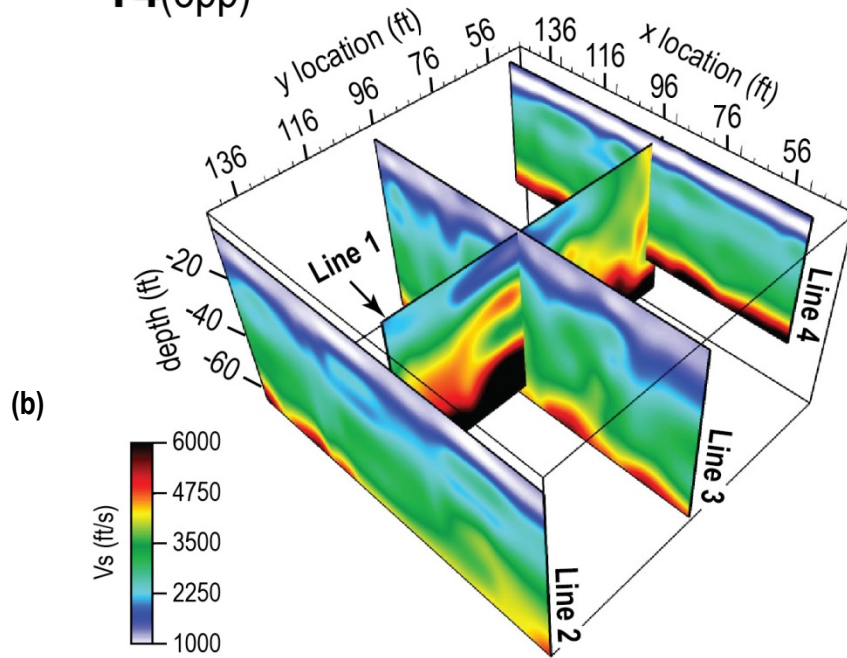


Figure D-4. Fence diagrams of 2-D V_s profiles at site T4 as viewed from (a) the perspective illustrated in Figure 8a, and (b) from the opposite (opp) corner of the site perimeter (Figure 8b).

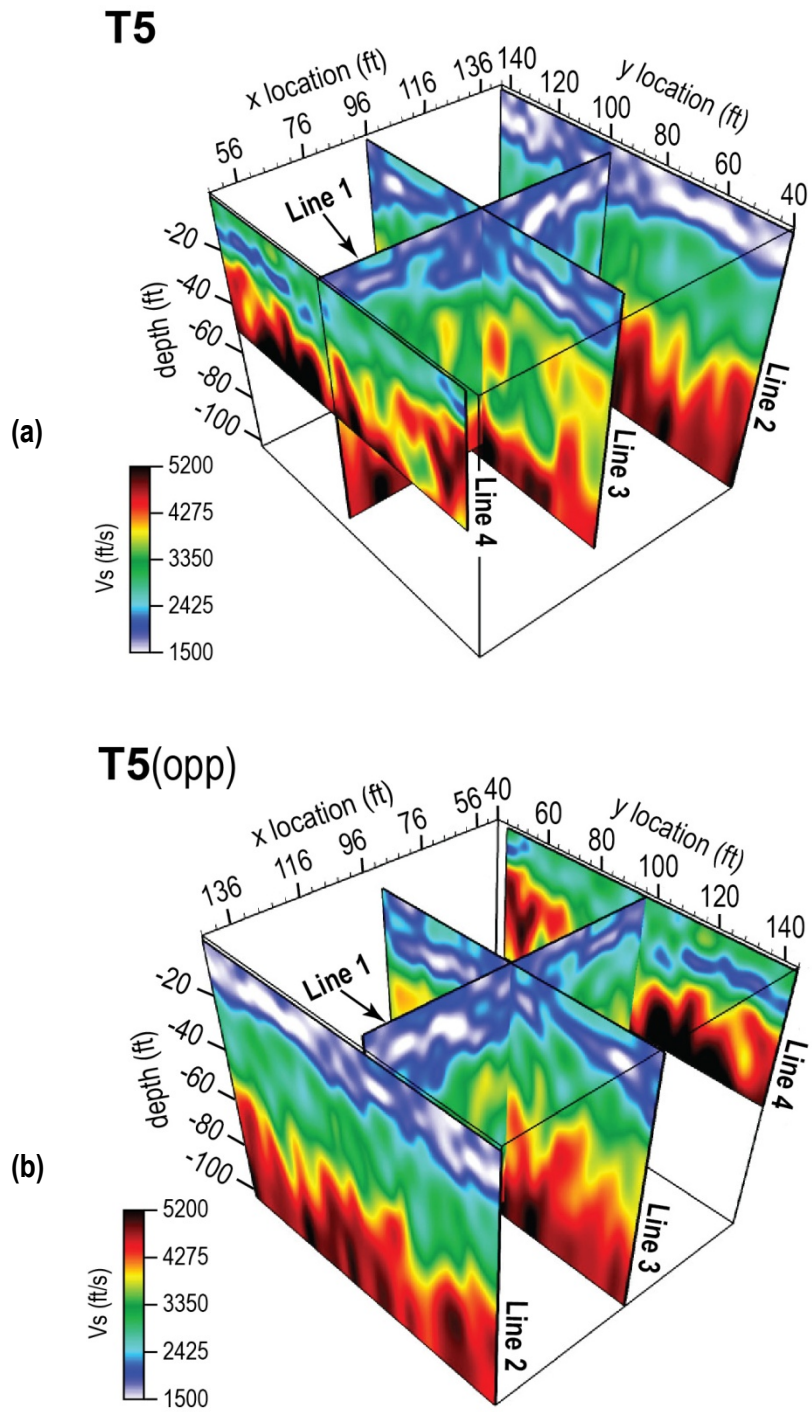


Figure D-5. Fence diagrams of 2-D Vs profiles at site T5 as viewed from (a) the perspective illustrated in Figure 8a, and (b) from the opposite (opp) corner of the site perimeter (Figure 8b).

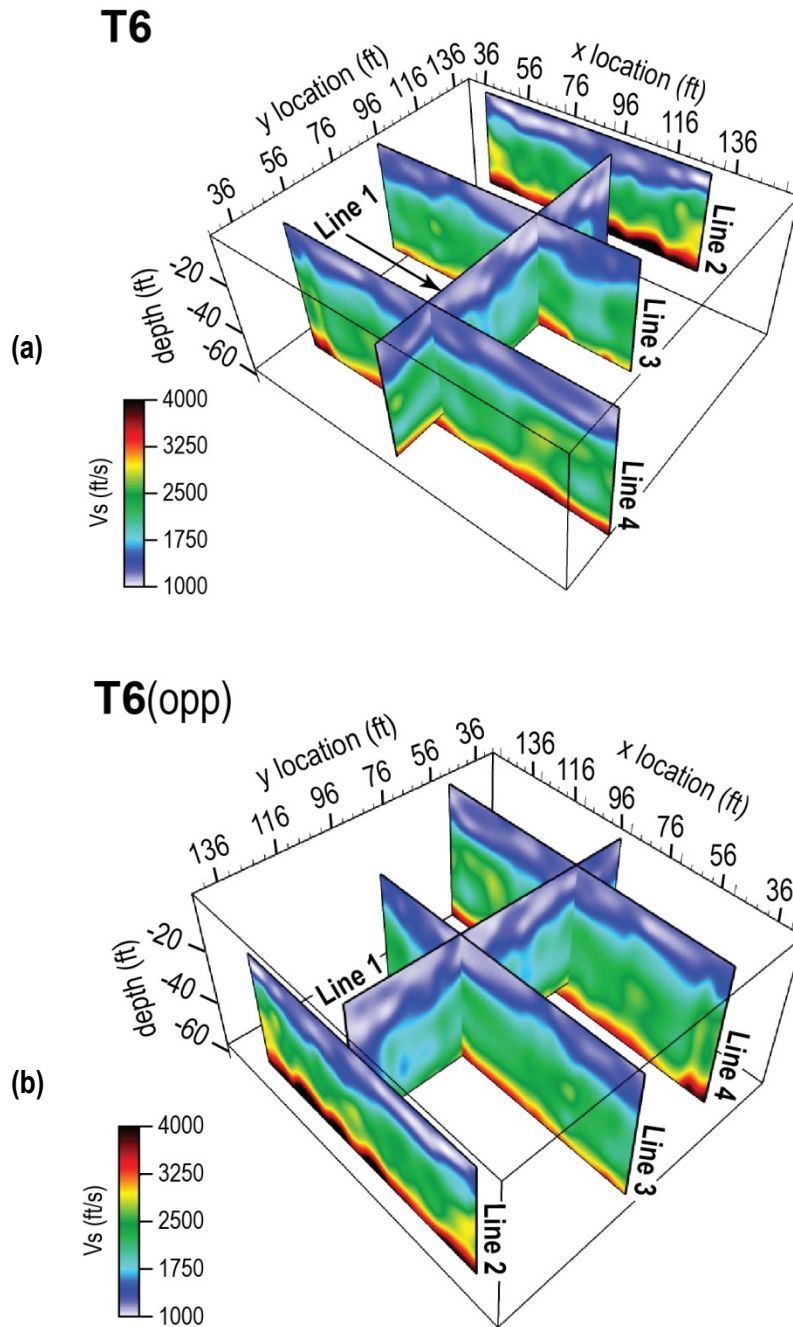
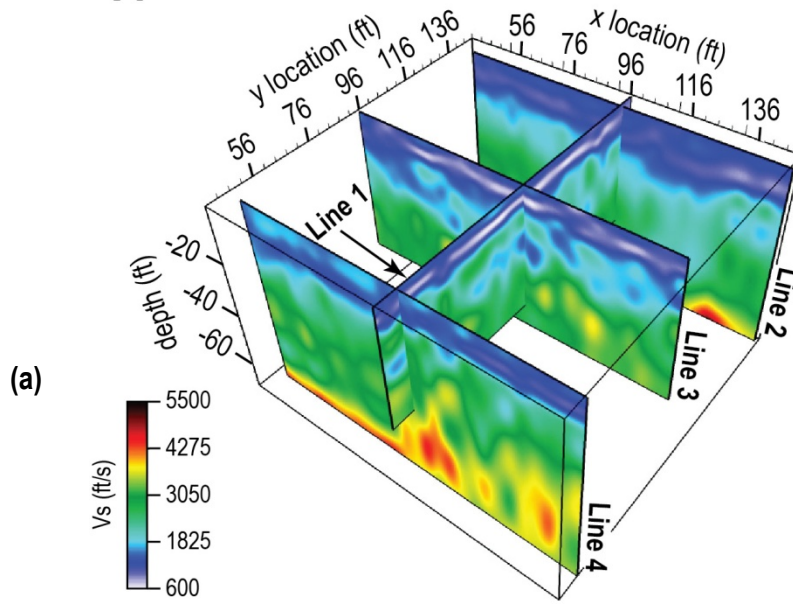


Figure D-6. Fence diagrams of 2-D V_s profiles at site T6 as viewed from (a) the perspective illustrated in Figure 8a, and (b) from the opposite (opp) corner of the site perimeter (Figure 8b).

T7



T7(opp)

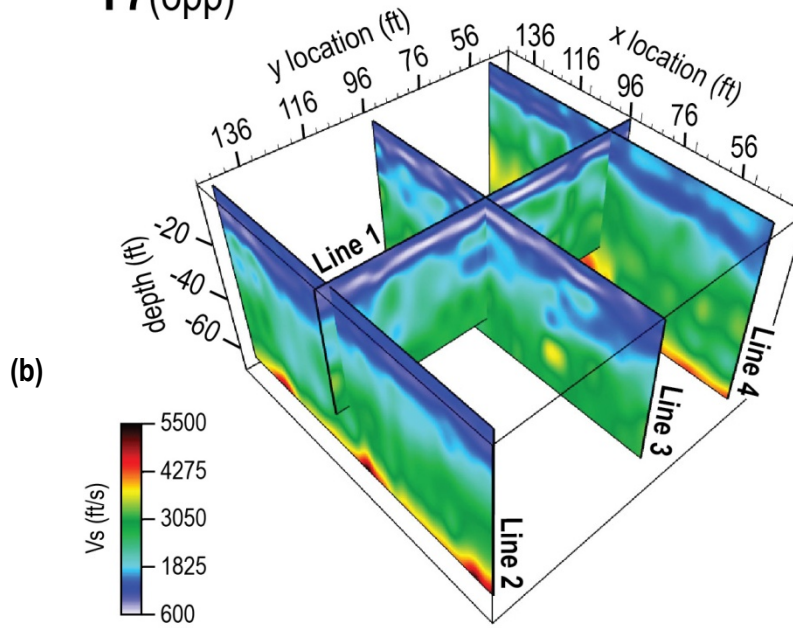


Figure D-7. Fence diagrams of 2-D V_s profiles at site T7 as viewed from (a) the perspective illustrated in Figure 8a, and (b) from the opposite (opp) corner of the site perimeter (Figure 8b).

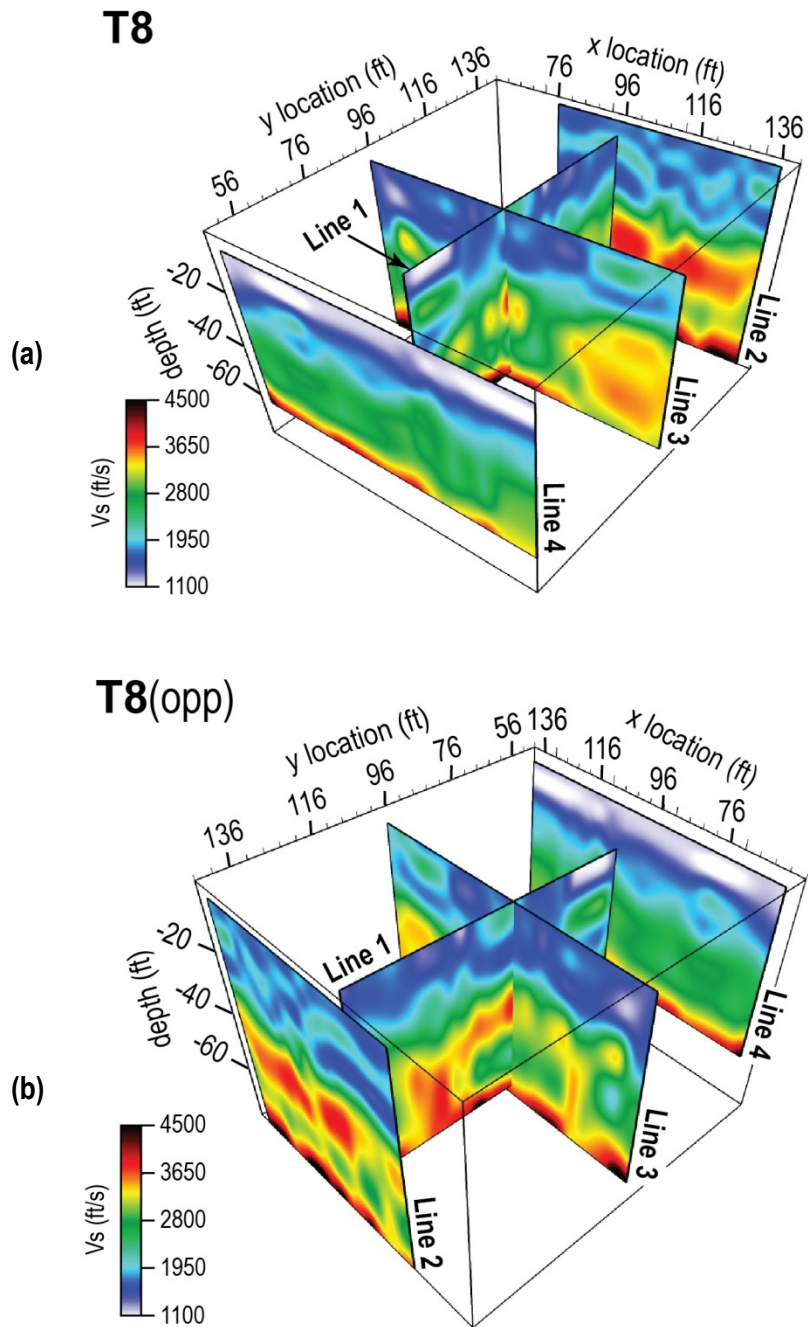


Figure D-8. Fence diagrams of 2-D Vs profiles at site T8 as viewed from (a) the perspective illustrated in Figure 8a, and (b) from the opposite (opp) corner of the site perimeter (Figure 8b).

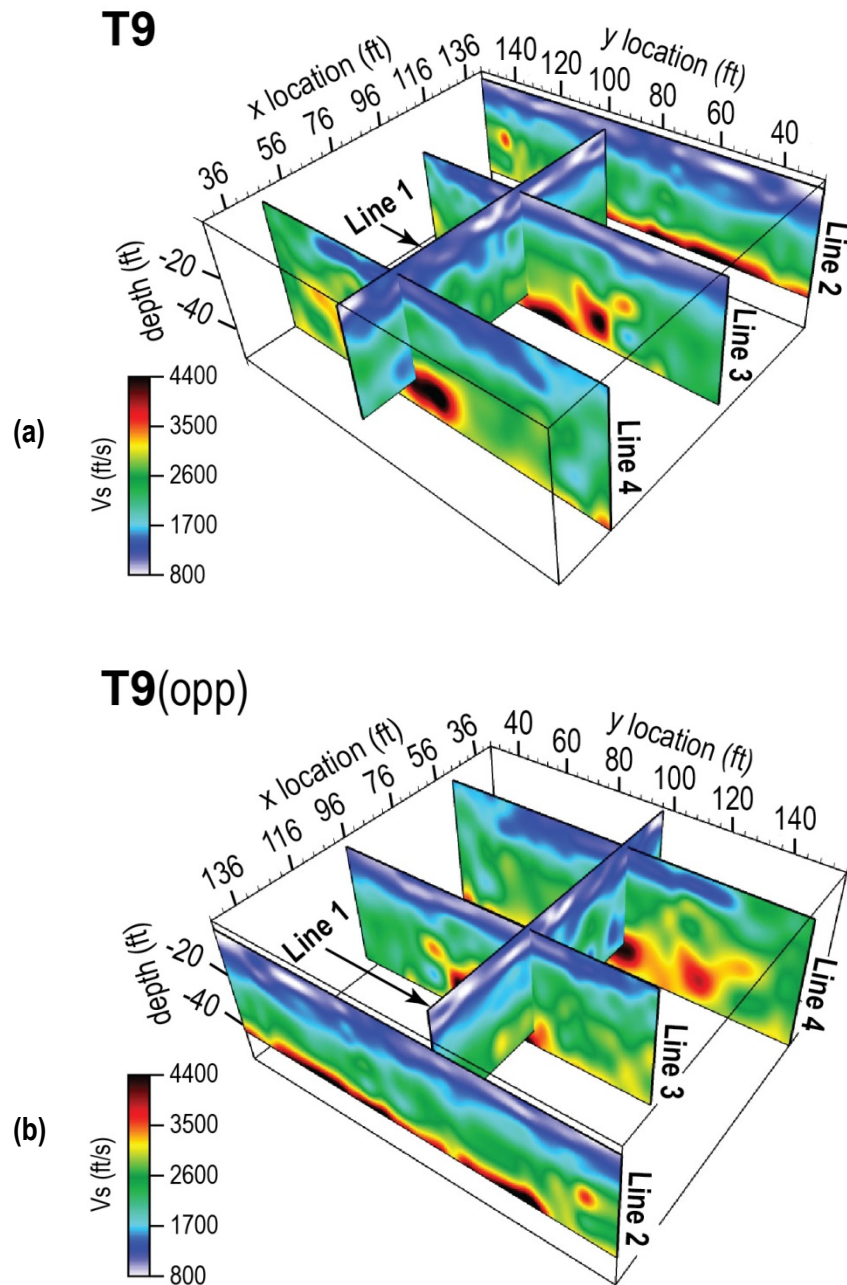


Figure D-9. Fence diagrams of 2-D V_s profiles at site T9 as viewed from (a) the perspective illustrated in Figure 8a, and (b) from the opposite (opp) corner of the site perimeter (Figure 8b).

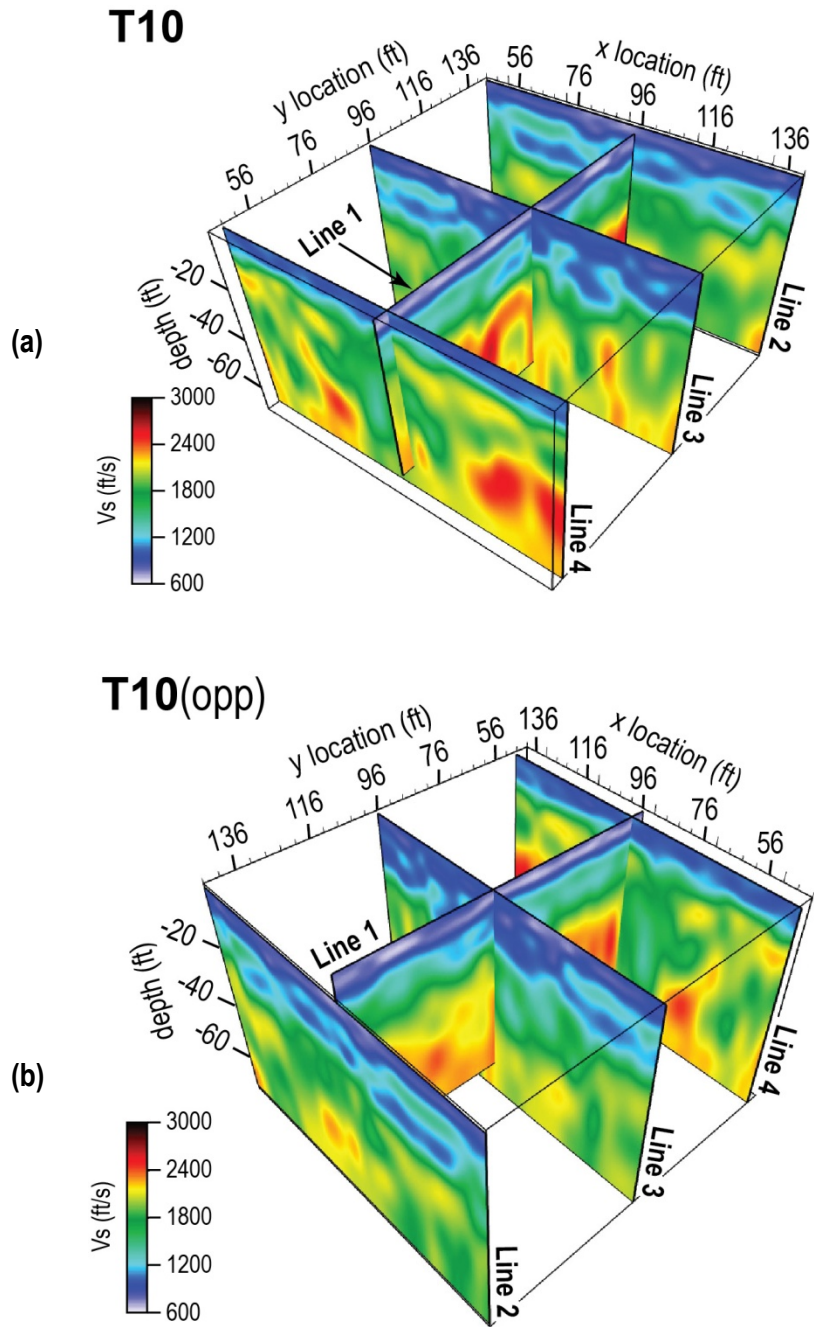


Figure D-10. Fence diagrams of 2-D V_s profiles at site T10 as viewed from (a) the perspective illustrated in Figure 8a, and (b) from the opposite (opp) corner of the site perimeter (Figure 8b).

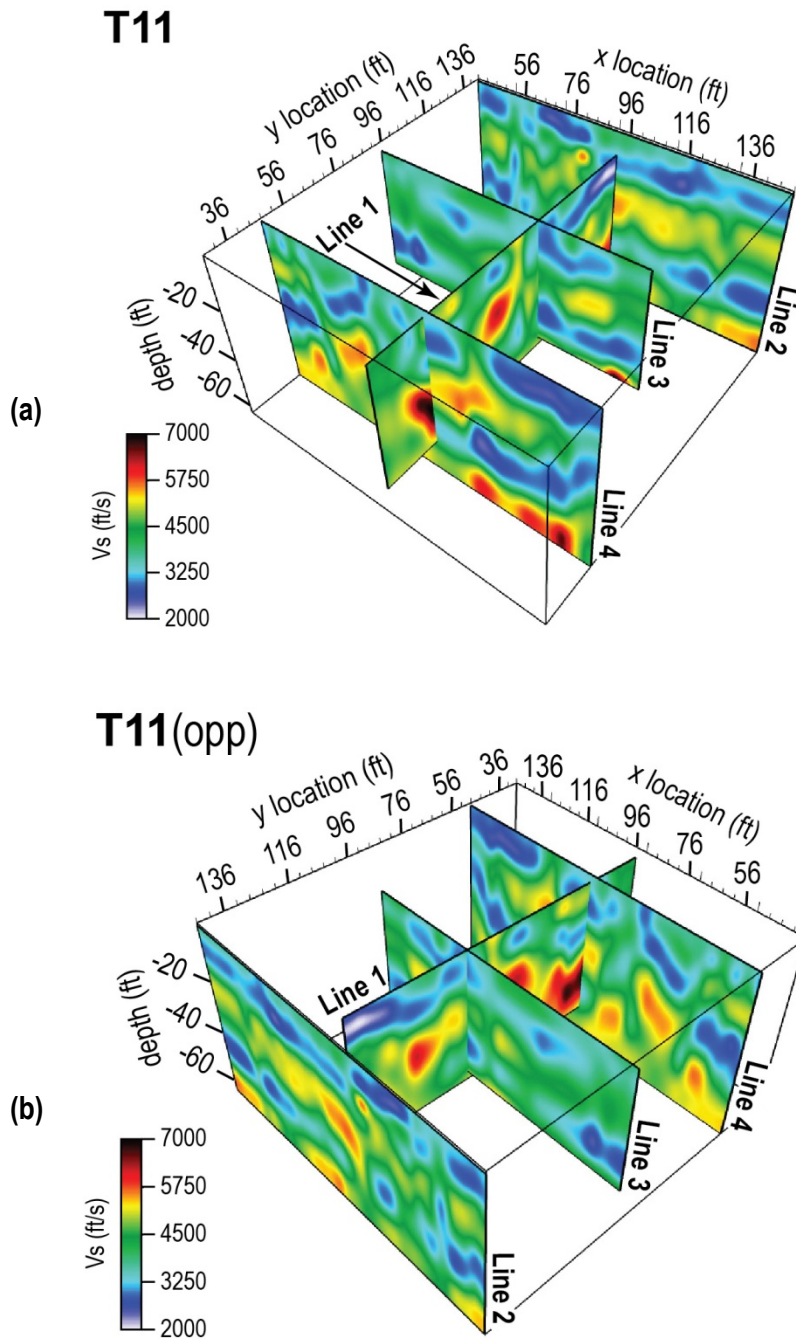


Figure D-11. Fence diagrams of 2-D Vs profiles at site T11 as viewed from (a) the perspective illustrated in Figure 8a, and (b) from the opposite (opp) corner of the site perimeter (Figure 8b).

APPENDIX E Isovelocity Surfaces

Note: isovelocity surfaces are viewed from the perspective illustrated in Figure 8a.

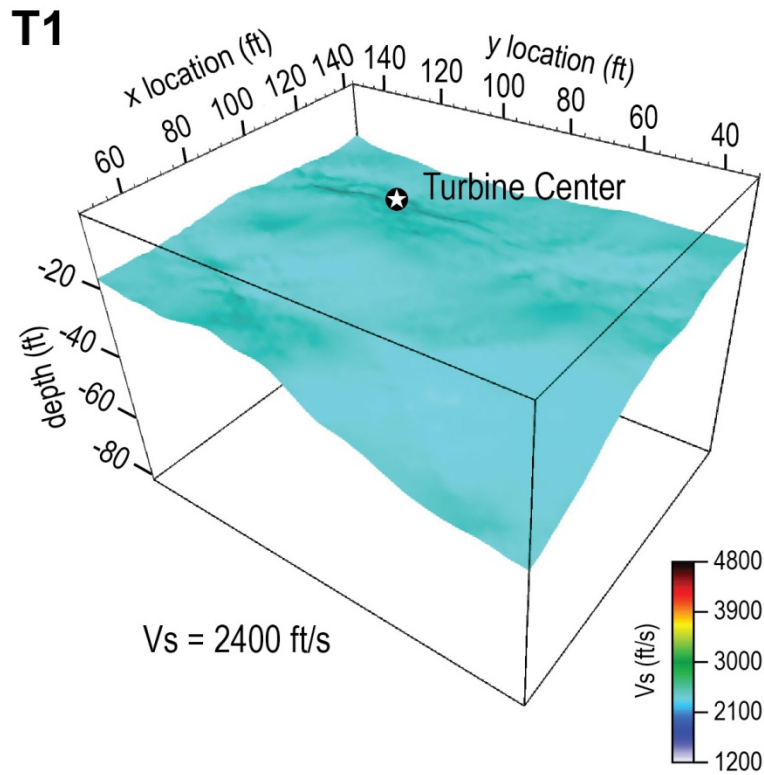


Figure E-1. Isovelocity surface defined by $V_s = 2400 \text{ ft/s}$ at site T1.

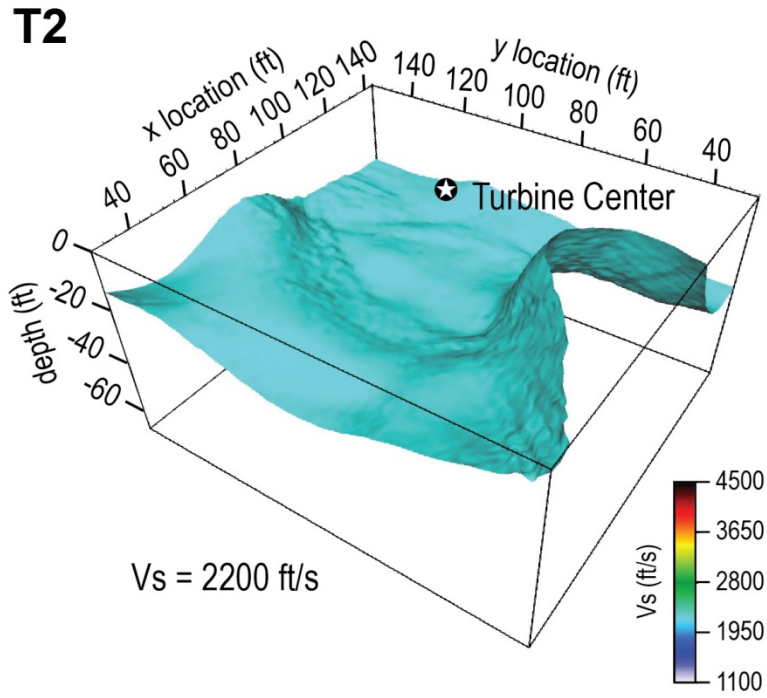


Figure E-2. IsovLOCITY surface defined by $V_s = 2200 \text{ ft/s}$ at site T2.

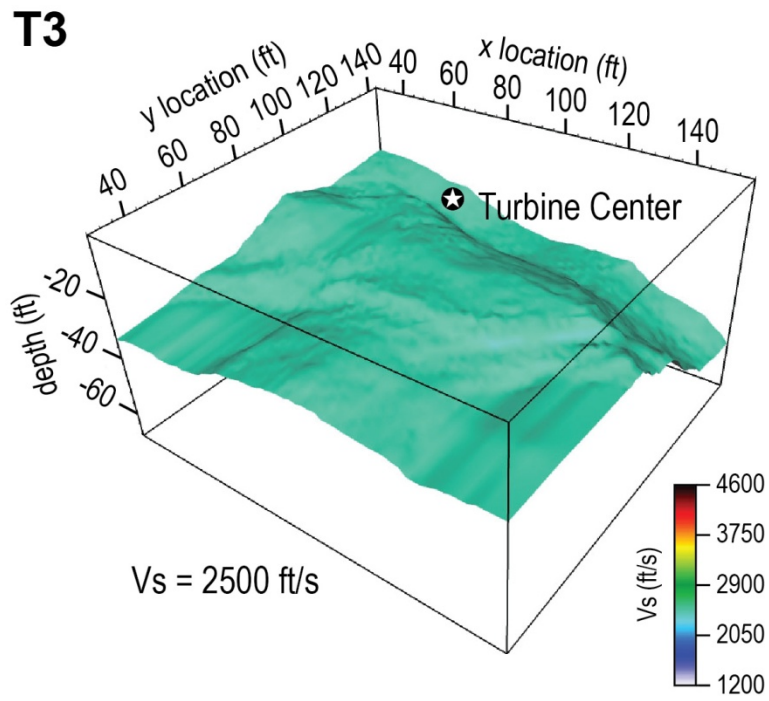


Figure E-3. IsovLOCITY surface defined by $V_s = 2500$ ft/s at site T3.

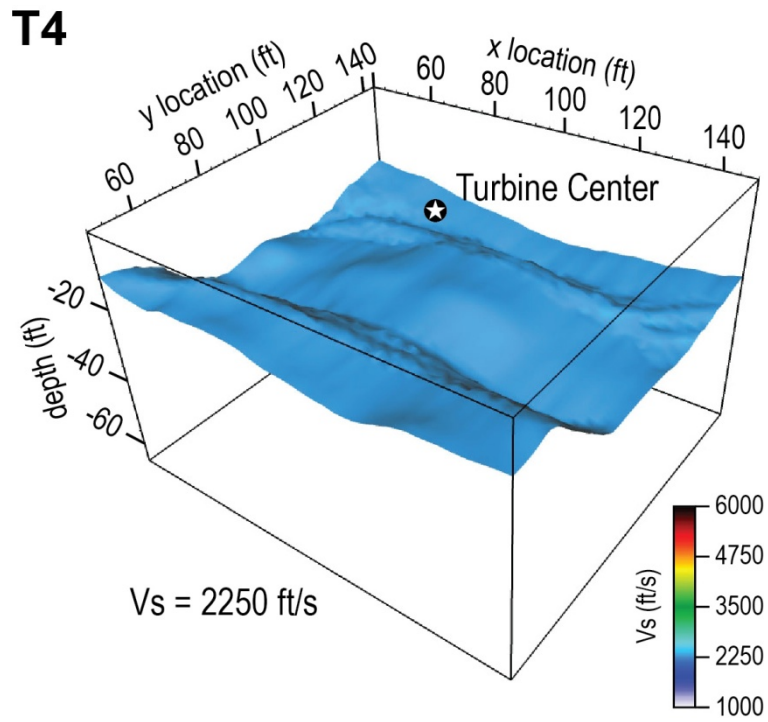


Figure E-4. Isovelocity surface defined by $V_s = 2250$ ft/s at site T4. The line 1 2-D V_s profile is not representative of the velocity of subsurface materials due to higher mode interference. Therefore, the line 1 profile was omitted from the 3-D rendering used to generate the isovelocity surface.

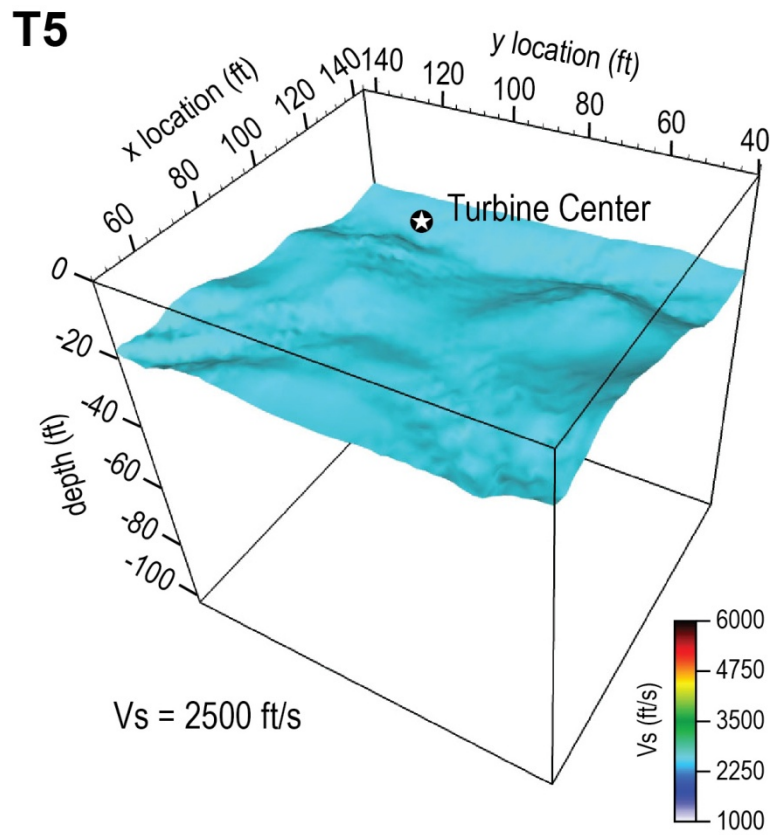


Figure E-5. Isovelocity surface defined by $V_s = 2400 \text{ ft/s}$ at site T5.

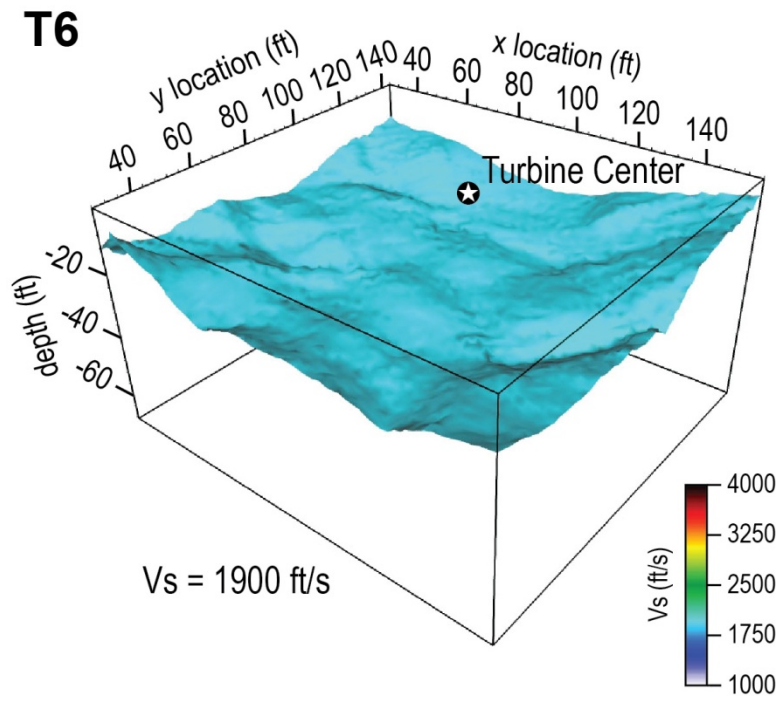


Figure E-6. Isovelocity surface defined by $V_s = 1900 \text{ ft/s}$ at site T6.

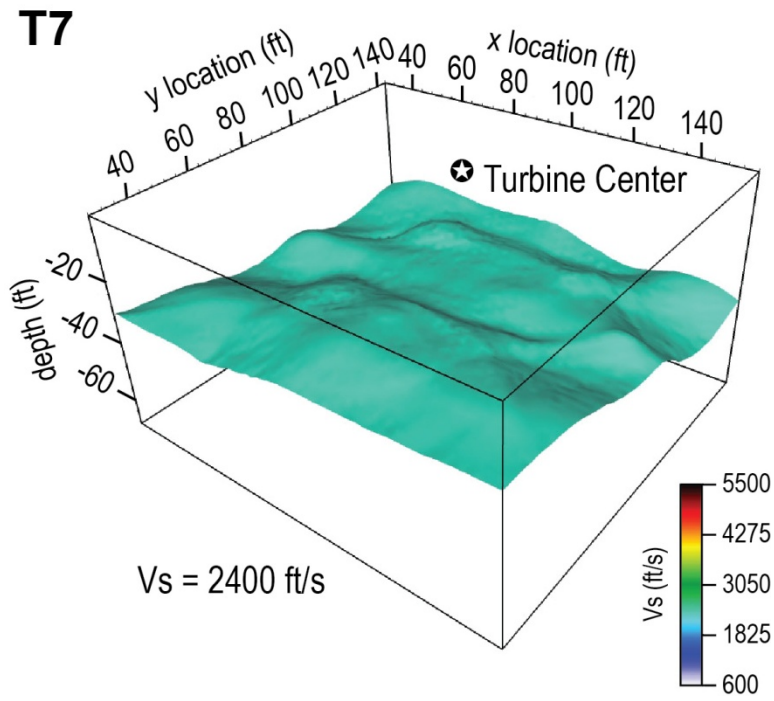


Figure E-7. Isovelocity surface defined by $V_s = 2400$ ft/s at site T7.

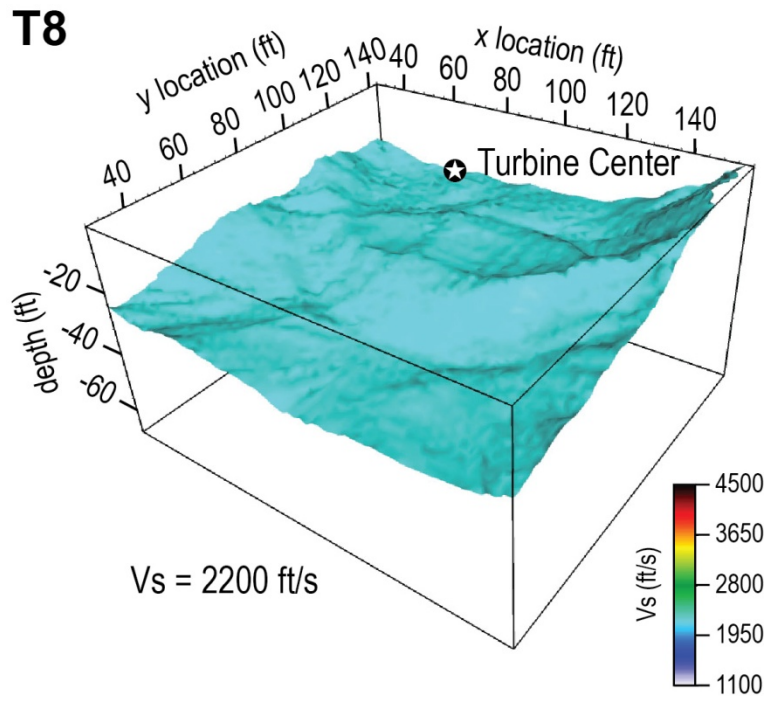


Figure E-8. Isovelocity surface defined by $V_s = 2200 \text{ ft/s}$ at site T8.

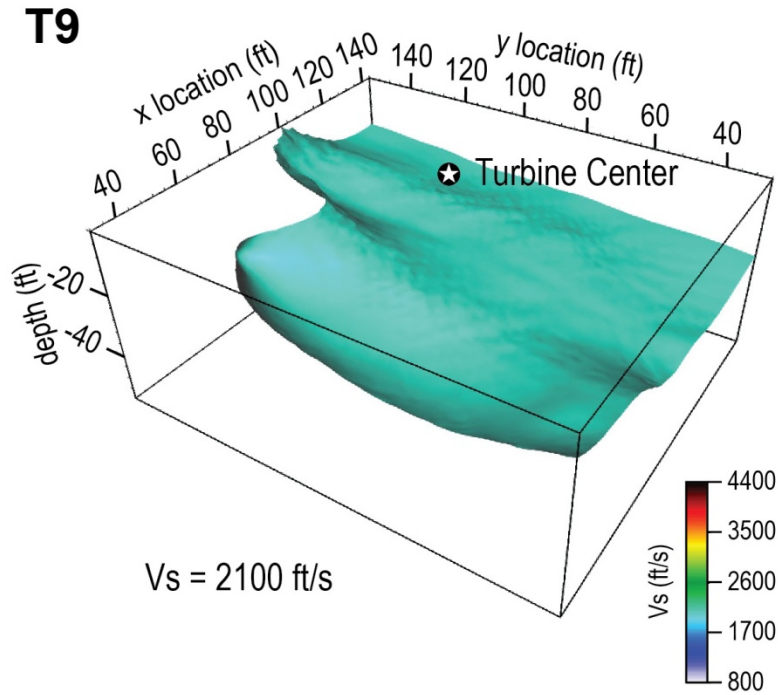


Figure E-9. Isovelocity surface defined by $V_s = 2100 \text{ ft/s}$ at site T9. V_s results suggest anisotropy at this site. Line 1 velocities would introduce an artificial depression in the isovelocity surface that is not representative of bedrock topography. Therefore, the line 1 profile was omitted from the 3-D rendering used to generate the isovelocity surface to preserve the approximate bedrock topography.

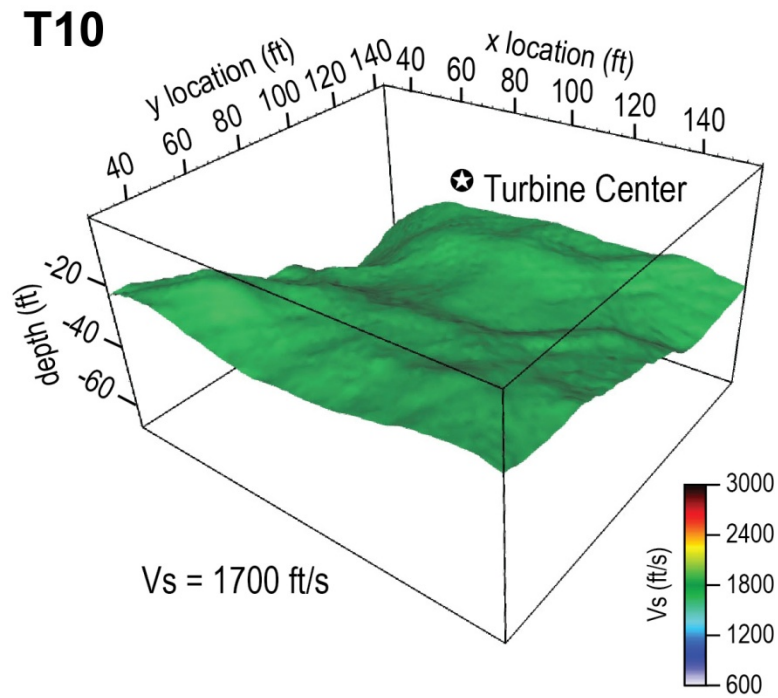


Figure E-10. Isovelocity surface defined by $V_s = 1700 \text{ ft/s}$ at site T10. V_s results suggest anisotropy at this site. Line 1 velocities would introduce an artificial rise in the isovelocity surface that is not representative of bedrock topography. Therefore, the line 1 profile was omitted from the 3-D rendering used to generate the isovelocity surface to preserve the approximate bedrock topography.

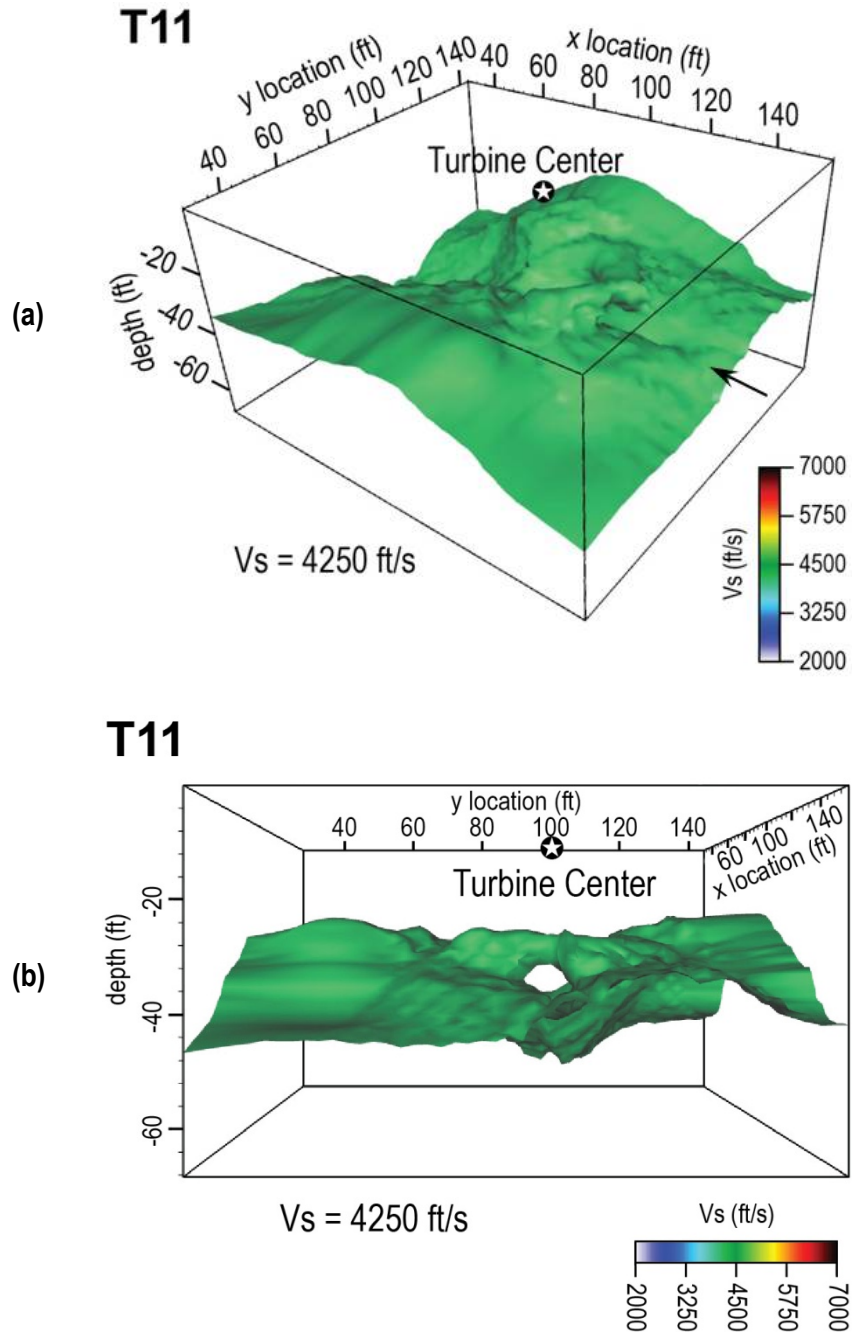


Figure E-11. Isovelocity surface defined by $V_s = 4250$ ft/s at site T11 as viewed from (a) the perspective illustrated in Figure 8a, and (b) as viewed in the direction of the arrow in (a). As evidenced by V_s obtained using MASW, bedrock at this site is at or near the surface. Therefore, a faster velocity was selected to delineate features beneath the bedrock surface at this site. Line 1 velocities would introduce an artificial rise in the isovelocity surface that is not representative of subsurface structure. Therefore, the line 1 profile was omitted from the 3-D rendering used to generate the isovelocity surface.